

1 **Passive acoustic monitoring from profiling floats as a pathway 2 to scalable autonomous observations of global surface wind**

3 Louise Delaigue¹, Pierre Cauchy², Dorian Cazau³, Julien Bonnel⁴, Sara Pensieri⁵, Roberto
4 Bozzano⁵, Anatole Gros-Martial⁶, Christophe Schaeffer⁷, Arnaud David⁷, Paco Stil¹, Antoine
5 Poteau¹, Catherine Schmechtig⁸, Edouard Leymarie¹ and Hervé Claustre¹

6 ¹Sorbonne Université, CNRS, Laboratoire d'Océanographie de Villefranche, LOV, 06230 Villefranche-sur-Mer,
7 France

8 ²Institut des sciences de la mer (ISMER), Université du Québec à Rimouski (UQAR), Rimouski, Québec, Canada

9 ³ENSTA, Lab-STICC, UMR CNRS 6285, Brest, France

10 ⁴Marine Physical Laboratory, Scripps Institution of Oceanography, University of California San Diego, La Jolla,
11 CA, 92093, USA

12 ⁵Institute for the Study of Anthropic Impact and Sustainability in the Marine Environment (IAS), Consiglio
13 Nazionale delle Ricerche (CNR), Genoa, Italy

14 ⁶Centre d'Études Biologiques de Chizé, CNRS, Villiers-en-bois, France

15 ⁷NKE Instrumentation, Hennebont, France

16 ⁸OSU Ecce Terra, UAR 3455, CNRS, Sorbonne Université, Paris Cedex, France

Deleted: 

17 *Correspondence to:* Louise Delaigue (louise.delaigue@imev-mer.fr)

18 **Abstract.** Wind forcing plays a pivotal role in driving upper-ocean physical and biogeochemical processes, yet
19 direct wind observations remain sparse in many regions of the global ocean. While passive acoustics have been
20 used to estimate wind speed from moored and mobile platforms, their application to profiling floats has been
21 demonstrated only in limited cases. Here we report the first deployment of a biogeochemical profiling float
22 equipped with a passive acoustic sensor explicitly designed for wind retrieval, aimed at detecting wind-driven
23 surface signals from depth. The float was deployed in the northwestern Mediterranean Sea near the DYFAMED
24 (DYnamique des Flux Atmosphériques en MEDiterranée) meteorological buoy from February to April 2025 and
25 operated at parking depths of 500–1000 m. We demonstrate that wind speed can be successfully retrieved from
26 subsurface ambient noise using established acoustic algorithms, with float-derived estimates showing good
27 agreement with collocated surface observations. To evaluate scalability to remote regions, we simulate a remote
28 deployment scenario by refitting the acoustic model of Nystuen et al. (2015) using ERA5 reanalysis as a reference
29 for surface wind. The ERA5-based calibration performs well under moderate winds but exhibits systematic high-
30 wind bias ($\geq 10 \text{ m s}^{-1}$). Finally, we apply a residual learning framework to correct these estimates using a limited
31 subset of DYFAMED wind data, simulating conditions where only brief surface observations are available. The
32 corrected wind time series achieved a 37% reduction in RMSE, demonstrating the effectiveness of combining
33 reanalysis with sparse in-situ calibration. This framework improves agreement with in-situ wind observations
34 relative to reanalysis alone, supporting a scalable strategy for float-based wind monitoring in data-sparse ocean
35 regions. Such capability has direct implications for improving estimates of air-sea exchanges, interpreting
36 biogeochemical fluxes, and advancing climate-relevant ocean observing.

Deleted: techniques

Deleted: and remains largely unexplored

Deleted: Here, we report on the first deployment of a profiling float equipped with a passive acoustic sensor

Deleted: , operating

Deleted: from the DYFAMED buoy

Deleted: the potential for broader application

Deleted: proxy

Deleted: Refitting the model to ERA5 data demonstrates that the float–acoustic–wind relationship is generalizable in moderate conditions, but high-wind regimes remain systematically biased—especially above

Deleted: —such as those from a ship during float deployment

Deleted: —

Deleted: and improved the coefficient of determination (R^2) from 0.85 to 0.91

Deleted: fitting

Deleted: This framework enables the retrieval of fine-scale wind variability not captured by reanalysis alone

Deleted: —with important implications for quantifying air-sea exchanges, improving biogeochemical flux estimates, and advancing global climate observations.

63 **1 Introduction**

64 Wind plays a fundamental role in driving ocean circulation, mediating air-sea gas exchange,
 65 and shaping climate-related biogeochemical processes (Wanninkhof, 2014; McGillicuddy,
 66 2016). Recent studies show that wind-driven circulation strongly influences regional climate
 67 trends (eg., Pelichero et al., 2020; Trenberth et al. 2025; McMonigal et al., 2025). Despite its
 68 central importance, accurately quantifying wind variability in remote ocean basins remains
 69 challenging. Satellite scatterometers suffer from coarse resolution, reduced performance under
 70 extreme weather and heavy cloud cover, and signal degradation in high-latitude regions, while
 71 surface moorings provide limited spatial coverage (Bentamy et al., 2003; Chelton et al., 2007;
 72 Stoffelen et al., 2008).

73 Passive acoustic monitoring of underwater ambient noise offers a complementary approach for
 74 inferring surface meteorological conditions from surface-generated underwater noise. The
 75 relationship between wind speed and high-frequency (1–20 kHz) noise generated by wave
 76 breaking and bubble entrainment has been extensively documented (Vagle et al., 1990; Farmer
 77 et al., 1998; Oguz and Prosperetti, 1990). This principle underpins the Weather Observations
 78 Through Ambient Noise (WOTAN) techniques and the development of Passive Acoustic
 79 Listener (PAL) instruments (Nystuen et al., 2001), enabling autonomous, long-term estimates
 80 of wind and rainfall from fixed and drifting platforms.

81 Although widely used, these approaches still face several limitations. The empirical
 82 relationships underpinning WOTAN-type methods are often site dependent, with deviations
 83 arising from bathymetry, wave regime, and water depth; even under wind-dominated
 84 conditions, shallow-water environments can yield substantially different spectral levels
 85 (Ingenito, 1989). Model skill is also limited by model design, as single-regime formulations
 86 underestimate the slope at higher winds and bias comparisons across SPL–wind relationships
 87 (Schwock, 2021). These factors complicate the selection of an appropriate empirical law for a
 88 given platform or region. To address these challenges, recent studies have explored data-driven
 89 and machine-learning approaches that learn wind–noise relationships directly from
 90 observations and reduce reliance on fixed empirical models (Taylor et al., 2020; Trucco et al.,
 91 2023; Zambra et al., 2023).

92 Despite these limitations the WOTAN framework has proven applicable across a wide range
 93 of platforms. Wind-driven signatures have been detected from moorings (Ma and Nystuen,
 94 2005; Nystuen et al., 2015; Pensieri et al., 2015), gliders (Cauchy et al., 2018; Cazau et al.,
 95 2019) and profiling floats (Riser et al., 2008; Yang et al., 2015; Yang et al., 2016; Bytheway
 96 et al., 2023; Ma et al., 2023), and even from biologged marine mammals operating in remote
 97 regions (Menze et al., 2013; Cazau et al., 2017; Gros-Martial et al., 2025a). Beyond wind
 98 estimation, acoustic sensors integrated into autonomous platforms have supported a wide range
 99 of geophysical and ecological applications, including marine mammal monitoring (Matsumoto
 100 et al., 2013; Cauchy et al., 2020; Fregosi et al., 2020; Baumgartner and Bonnel, 2022), and
 101 hydroacoustic earthquake detection and characterisation of ambient ocean noise (Baumgartner
 102 et al., 2017; Pipatprathanporn and Simons, 2022).

103 Recognising this broad utility, the Ocean Sound Essential Ocean Variable (EOV), coordinated
 104 by the International Quiet Ocean Experiment (IQOE) and endorsed by the Global Ocean
 105 Observing System (GOOS), identifies autonomous platforms such as profiling floats as ideal

- Deleted:** dynamics
- Deleted:** fluxes of gases and governing biological productivity
- Deleted:** modelling
- Deleted:** emphasize
- Deleted:** ocean
- Deleted:** significantly
- Deleted:** , such as the North Atlantic Warming Hole phenomenon
- Formatted:** English (US)
- Deleted:** critical
- Deleted:** oceanic
- Deleted:** remains challenging, particularly
- Deleted:** and undersampled regions such as the Southern Ocean, where
- Deleted:** s
- Deleted:** retrievals are limited by
- Deleted:** signal degradation from storms,
- Deleted:** sea ice
- Deleted:** Consequently, observational gaps persist, affecting our understanding of critical processes like air-sea carbon exchange during storm events (Carranza et al., 2024).^[1]
- Deleted:** Traditionally, oceanic wind observations have relied heavily on satellite scatterometry and surface-based platforms, including meteorological buoys. (Chelton et al., 2007; Verhoef et al., 2012) While scatterometers provide near-global wind observations, their effectiveness diminishes significantly under stormy conditions, heavy precipitati^[2]
- Moved up [1]:** (Chelton et al., 2007; Verhoef et al., 2012)
- Moved (insertion) [1]**
- Deleted:** p
- Deleted:** sensing
- Deleted:** generated by surface wind stress and wave-^[3]
- Deleted:** ambient
- Deleted:** (1–20 kHz)
- Deleted:** validated through theoretical and empirical studies
- Deleted:** These foundational studies demonstrated tha^[4]
- Deleted:** .
- Formatted:** English (US)
- Moved (insertion) [3]**
- Deleted:** Yang et al., 2015; Yang et al., 2016Cazau et^[5]
- Formatted:** English (US)
- Formatted**^[6]
- Formatted**^[7]
- Deleted:** This approach builds on the Weather Observa^[8]

184 platforms for distributed global acoustic monitoring (Tyack et al., 2023). In recent decades,
 185 biogeochemical (BGC)-Argo floats have become a central component of global ocean
 186 observing systems. Their persistence at sea, broad spatial coverage, and cost-effectiveness have
 187 demonstrated clear advantages over traditional ship-based measurements (Roemmich et al.,
 188 2009; Riser et al., 2016). As their capabilities have expanded, these platforms now host
 189 increasingly sophisticated multidisciplinary sensor suites, with measurements of oxygen,
 190 nitrate, chlorophyll, pH, and irradiance (Johnson and Claustre, 2016; Claustre et al., 2020). Yet,
 191 despite this progress, the integration of passive acoustics into BGC-Argo remains largely
 192 unexplored. Incorporating acoustic wind sensing would supply the atmospheric forcing needed
 193 to interpret biogeochemical variability, particularly in high-latitude or storm-dominated
 194 regions where wind products remain sparse or uncertain.

195 Here, we present the first deployment of a biogeochemical profiling float equipped with a
 196 passive acoustic sensor explicitly designed for wind speed estimation from underwater ambient
 197 noise. Deployed in the northwestern Mediterranean Sea, near the DYFAMED (DYnamique
 198 des Flux Atmosphériques en Méditerranée) meteorological buoy, this float serves as a proof-
 199 of-concept demonstration to: (1) determine whether wind-driven acoustic signatures can be
 200 detected at profiling float parking depths; (2) evaluate the performance of established acoustic
 201 wind models on this platform; and (3) develop a practical framework combining acoustic
 202 observations with reanalysis data and machine learning to enable wind estimation in remote
 203 regions. Through this approach, we demonstrate the potential of acoustic-equipped profiling
 204 floats to expand global wind observations, close persistent observational gaps, and support
 205 interpretation of biogeochemical and climate-relevant processes.

Deleted: Advancements in passive acoustic sensing technology have enabled the integration of acoustic sensors onto autonomous oceanographic platforms, including underwater gliders (Cazau et al., 2018; Cauchy et al., 2018) and profiling floats equipped with PAL sensors (Riser et al., 2008; Yang et al., 2015; Yang et al., 2016; Ma et al., 2023). Such developments are especially valuable in remote environments, where traditional in-situ measurements remain limited. For example, Menze et al. (2012) provided early evidence of wind-dependent acoustic noise regimes in ... [9]

Moved up [3]: Cazau et al., 2018; Cauchy et al., 2018

Moved up [4]: Yang et al., 2015; Yang et al., 2016

Formatted: Default Paragraph Font, Font color: Auto, English (UK)

Formatted: Default Paragraph Font, Font color: Auto, English (UK)

Formatted: Default Paragraph Font, Font color: Auto, English (UK)

Formatted: Default Paragraph Font, Font: Times New Roman, 12 pt, Font color: Auto, English (UK)

Formatted: Font: Times New Roman, 12 pt, Font color: Auto, English (UK)

Formatted: Default Paragraph Font, Font color: Auto, English (UK)

Formatted: Font: Times New Roman, 12 pt, Font color: Auto, English (UK)

Moved (insertion) [2]:

Deleted: Despite these advancements, integration of passive acoustic sensors onto modern biogeochemical (BGC) ... [10]

Moved up [2]: The integration of acoustic sensors into BGC-Argo floats thereby holds promise for closing

Deleted: Recent technological developments, including low-power acoustic sensors optimised for integration ... [11]

Deleted: In this study, we present the first deployment of a profiling float equipped with a passive acoustic sensor ... [12]

Deleted: by integrating advanced acoustic sensing with simultaneous biogeochemical measurements.

Formatted: Default Paragraph Font, Font color: Auto, English (UK)

Formatted: Default Paragraph Font, Font color: Auto, English (UK)

Formatted: Default Paragraph Font, Font color: Auto, English (UK)

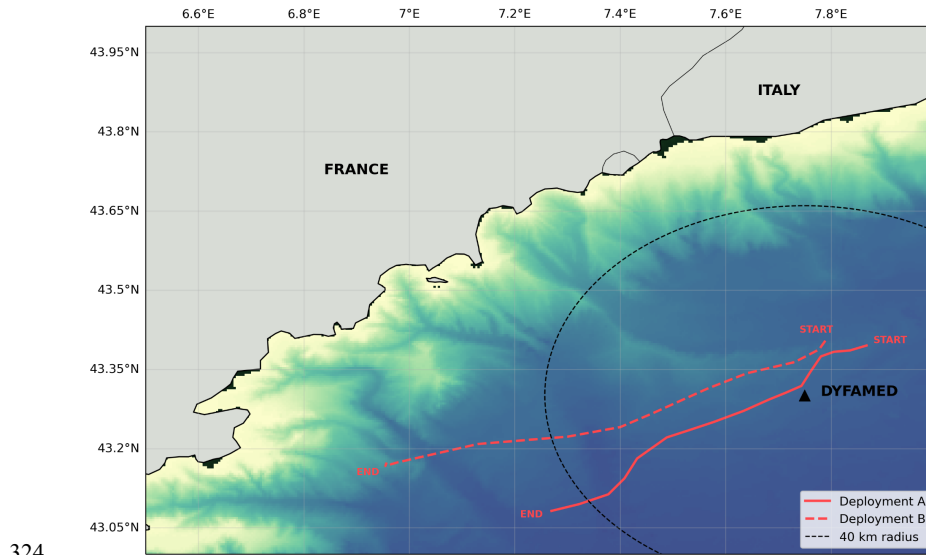
Formatted: Default Paragraph Font, Font color: Auto, English (UK)

Formatted: Default Paragraph Font, Font color: Auto, English (UK)

Formatted: Default Paragraph Font, Font color: Auto, English (UK)

Formatted: Font: Times New Roman, 12 pt, Font color: Auto, English (UK)

Deleted: Our main objective is to assess the feasibility and precision of acoustic-based wind retrieval methods by ... [13]

323 **2 Materials and Methods**

324 **Figure 1.** Float trajectories during sea trials conducted in the Ligurian Sea in February and
 325 March 2025. Deployment A (solid line) and Deployment B (dashed line) are shown along with
 326 a concentric dashed circle (40 km radius) centred on the DYFAMED station. The 40 km radius
 327 was used to spatially filter float data for refitting and validation of wind estimates at
 328 DYFAMED, as described in Cauchy et al. (2018).
 329

330 **2.1 Study area and DYFAMED weather station**

331 The acoustic wind sensing trial was conducted in the Ligurian Sea, a sub-basin of the
 332 northwestern Mediterranean, in proximity to the DYFAMED (DYnamique des Flux
 333 Atmosphériques en MEditerranée) oceanographic time series station (Fig. 1). This station is
 334 part of the national observation program MOOSE (Mediterranean Ocean Observing System
 335 for the Environment, <https://www.moose-network.fr>, funded by CNRS-INSU, and has been
 336 integrated since 2016 into the national research infrastructure ILICO (Infrastructure de
 337 recherche littorale et côtière; Cocquempot et al., 2019).

338 Located at 43.42°N, 7.87°E, DYFAMED has served as a key reference site for air-sea
 339 exchange, upper ocean dynamics, and biogeochemical cycling since the early 1990s. The site
 340 is equipped with continuous meteorological and oceanographic monitoring, including high-
 341 quality wind speed and direction measurements from the Côte d'Azur meteorological
 342 buoy, operated by Météo-France, located at the DYFAMED site. These data are reported at
 343 hourly resolution following WMO (World Meteorological Organization) standards and include
 344 wind parameters, air temperature, pressure, humidity, and sea state.

Formatted: Font: Times New Roman, 12 pt, Font color: Auto, English (UK)

Formatted: Default Paragraph Font, Font color: Auto, English (UK)

Formatted: Default Paragraph Font, Font: Not Bold, Font color: Auto, English (UK)

Formatted: Default Paragraph Font, Font color: Auto, English (UK)

Formatted: Default Paragraph Font, Font color: Auto, English (UK)

Formatted: Default Paragraph Font, Font color: Auto, English (UK)

Formatted: Default Paragraph Font, Font color: Auto, English (UK)

Formatted: Default Paragraph Font, Font: Times New Roman, 12 pt, Font color: Auto, English (UK)

Deleted: (43.42°N, 7.87°E)

Formatted: Font: Times New Roman, 12 pt, Font color: Auto, English (UK)

Formatted: Default Paragraph Font, Font color: Auto, English (UK)

Formatted: Default Paragraph Font, Font: Times New Roman, 12 pt, Font color: Auto, English (UK)

Formatted: Default Paragraph Font, Font color: Auto, English (UK)

Formatted: Default Paragraph Font, Font: Times New Roman, 12 pt, Font color: Auto, English (UK)

Formatted: Default Paragraph Font, Font color: Auto, English (UK)

Formatted: Default Paragraph Font, Font color: Auto, English (UK)

Formatted: Default Paragraph Font, Font color: Auto, English (UK)

346 During the study period, wind speeds at DYFAMED ranged from 0.5 to 16.1 m s⁻¹, with a mean
 347 of 6.8 m s⁻¹ and a measurement precision of one decimal place.

348 **2.2 Acoustic sensor integration**

349 The float used in this study was equipped with a passive acoustic module jointly developed by
 350 NKE and ABYSsens in collaboration with LOV. This module was specifically designed for
 351 integration into the PROVOR CTS5 BGC-Argo platform, with the aim of minimizing power
 352 consumption and data volume while remaining compatible with the operational constraints of
 353 the BGC-Argo program.

354 The module consists of two main parts enclosed in a dedicated external housing: 1) a low-noise
 355 HTI-96-Min hydrophone (sensitivity: -165 dB re 1 V/µPa; frequency range: 2 Hz–30 kHz),
 356 mounted externally to capture pressure fluctuations, and 2) an ABYSsens acquisition board,
 357 which conditions, digitizes, and processes the signal.

358 The acquisition system operates in a low-power pulsed mode (220 mW) with a sampling
 359 frequency up to 62.5 kHz and 24-bit resolution. To limit power usage and transmission needs,
 360 raw acoustic signals are not stored. Instead, the sensor performs direct onboard integration into
 361 23 third-octave bands, spanning from 63 Hz to 25 kHz with a variable integration time (see
 362 Table 1). Higher-frequency bands (e.g., 3.15–25 kHz) used shorter integration times (50 ms),
 363 while low-frequency bands used longer windows (up to 500 ms).

Frequency band range	Integration time
<u>63</u> , 100, <u>125</u> and 160 Hz	500 ms
400 , 500 and 630 Hz	250 ms
800 Hz, <u>1</u> , 1.25, 1.6, <u>2</u> and 2.5 kHz	100 ms
3.15, 4, <u>5</u> , 6.3, <u>8</u> , 10, <u>12.5</u> , 16, <u>20</u> and 25 kHz	50 ms

364 **Table 1.** Integration times applied to third-octave bands during acoustic signal processing,
 365 varying by frequency range to balance energy and spectral accuracy. In bold and underlined,
 366 the bands transmitted in the 9-band float configuration.

367 The acoustic unit is mounted on the upper section of the float chassis and is configured to
 368 operate exclusively during the parking phase (500–1000 m depth; Fig. 3). During this phase,
 369 the float drifts with only routine background measurements (e.g., pressure, CTD), and acoustic
 370 acquisition is automatically suspended whenever noisy operations such as ballast pumping or
 371 CTD sampling occur, thereby avoiding contamination from self-noise.

372 The float system allows for flexible and modifiable configuration via satellite: the user can
 373 define the number of bands transmitted (23, 9, or a compact onboard estimate of wind/rain),

Deleted: The station is equipped with continuous meteorological and oceanographic monitoring, including high-quality wind speed and direction measurements from a surface buoy maintained by Météo-France. These data are reported at hourly resolution, following WMO (World Meteorological Organization) standards, and include wind parameters, along with air temperature, pressure, humidity, and sea state.

Formatted: Justified

Formatted: Justified

Formatted: Justified

Formatted: Justified

Formatted: Justified

Deleted: “

Deleted:

Deleted: s”

385 the acquisition interval (typically 5–15 minutes), and the number of acoustic samples averaged
 386 per measurement. In this study, we used a 5-minute interval with 10 averaged acquisitions per
 387 measurement (each acquisition is a spectral estimation using the integration times defined in
 388 Table 1).

389 The telemetry and energy impact of adding an acoustic sensor to a 6-variable biogeochemical
 390 float was evaluated by using the programming interface provided by NKE. The estimated
 391 reduction in the number of cycles varies from 18% for acquisition every 5 minutes to 7% for
 392 acquisition every 15 minutes during the whole parking drift of a 10-day Argo cycle and with 5
 393 averaged acquisitions per acoustic measurement. The data volume increase depends on the
 394 transmission format: from ~9% for onboard wind–rain estimates (15-min period) to ~85% for
 395 a full 23-band spectrum (5-min period). A 9-band spectrum every 15 minutes—a likely
 396 recommended setup—adds ~16%. These overheads remain within the platform’s capacity,
 397 confirming compatibility with concurrent BGC measurements.

398 Each sensor output transmitted by the float corresponds to the Third Octave Level (TOL), i.e.,
 399 the sound pressure level integrated over a third-octave band, expressed in dB re 1 μ Pa. These
 400 TOLs represent the float’s primary spectral product and are used as input to the wind speed
 401 retrieval models. The amplitude resolution of the transmitted data is 0.2 or 0.5 dB, with a
 402 dynamic range up to 127 dB. This discretisation arises because the data are transmitted as
 403 integers to save bandwidth, which requires selecting a resolution step.

404 2.3 Depth correction and spectral normalization

405 To account for the attenuation of surface-generated noise with depth, a correction term $\beta(h,f)$
 406 was applied to all acoustic measurements (Fig. 2). Because β depends on the ambient
 407 temperature–salinity structure, we quantified hydrographic stability over the 60-day
 408 deployment using all profiles that reached at least 1000 dbar. Each profile was interpolated
 409 onto a 1 m grid and compared to the deployment-mean temperature/salinity profiles. Depth-
 410 averaged RMS deviations were $0.14 \pm 0.04^\circ\text{C}$ for temperature and 0.06 ± 0.02 for salinity, and
 411 no profile exceeded $|z| = 2$ standardised deviation, confirming weak hydrographic variability.
 412 Because such differences are far below hydrophone measurement uncertainties, $\beta(h,f)$ was
 413 computed once using the deployment-mean profile and applied uniformly to the full record.
 414 For longer or more dynamic missions, $\beta(h,f)$ should be recomputed for each profile. Modern
 415 hardware makes this operation computationally inexpensive, but the negligible hydrographic
 416 variability in this deployment renders repeated recalculation unnecessary.

417 Following Cauchy et al. (2018), the correction takes the form:

$$418 \text{TOL}_0(f) = \text{TOL}(h,f) + \beta(h,f) \quad (1a),$$

$$419 \text{where } \beta(h,f) = -10 \log \left\{ 2 \int_0^{\infty} \left[\frac{r \sin^2 \theta_{r,h} e^{-\alpha_f l_{r,h}}}{l^2_{r,h}} \right] dr \right\} \quad (1b),$$

Formatted: Font: Times New Roman, 12 pt, Font color: Auto, English (UK)

Formatted: Font: Times New Roman, 12 pt, Font color: Auto, English (UK)

Formatted: Font: Times New Roman, 12 pt, Font color: Auto, English (UK)

Formatted: Font: Times New Roman, 12 pt, Font color: Auto, English (UK)

Formatted: Font: Times New Roman, 12 pt, Font color: Auto, English (UK)

Formatted: Font: Times New Roman, 12 pt, Font color: Auto, English (UK)

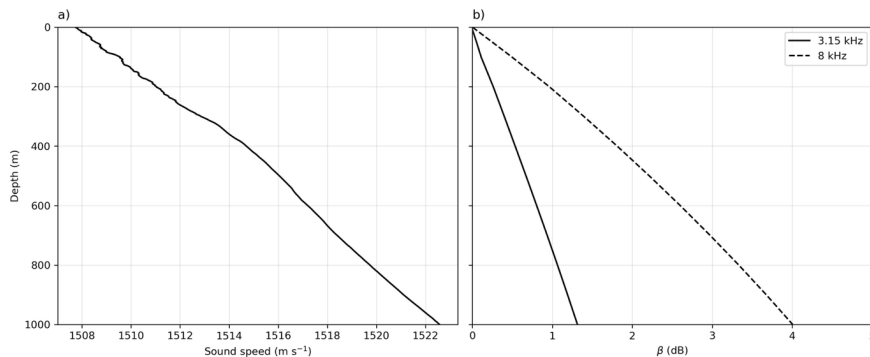
Deleted: To account for the attenuation of surface-generated noise with depth, a correction was applied to all acoustic measurements (Fig. 2). In this study, the correction term was calculated from the first temperature–salinity profile (Fig. 2a-b) and applied throughout the deployment, as the float remained in relatively stable hydrographic conditions (Fig. 2c). For long-term or basin-scale missions, however, this coefficient would need to be recomputed for each profile, since temperature and salinity variability along the float trajectory can significantly affect sound propagation.¶

428 with $TOL(h, f)$ as the raw TOL measurement from the profiling float, h as the sensor depth, f
 429 the centre frequency of the band, r the horizontal distance from a surface noise source to the
 430 point vertically above the sensor, l the total pathlength between source and receiver (accounting
 431 for depth and refraction), including refraction effects, θ the angle between the emitted acoustic
 432 ray and the horizontal axis, and α the frequency-dependent attenuation coefficient for bubble-
 433 free water. The integral considers contributions from all surface-generated acoustic sources
 434 over the sea surface, assuming radial symmetry, and accounts for geometric spreading,
 435 frequency-dependent absorption, and angle-dependent energy emission along each path. This
 436 correction was originally derived for third-octave levels and is directly applicable here, as the
 437 float outputs TOLs at fixed centre frequencies.

438 Then, depth-corrected third-octave levels $TOL_0(f)$ (dB re 1 μ Pa) were converted to spectral
 439 density levels $SPL(f)$ (dB re 1 μ Pa/Hz) by normalising to the bandwidth of each band. In the
 440 following, SPL always refers to these depth-corrected, bandwidth-normalised values derived
 441 from $TOL_0(f)$. This step ensures consistency across frequencies and comparability with model
 442 spectra. In future deployments, this spectral correction will be applied directly onboard the
 443 float.

Deleted: in

Formatted: Justified

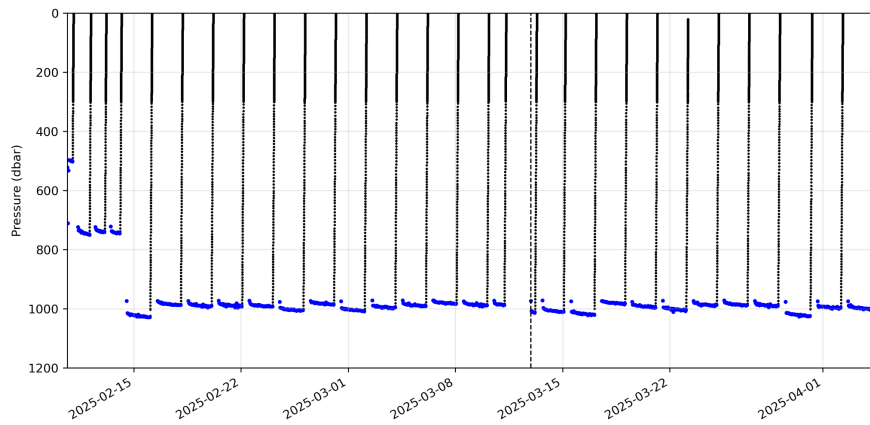


444
 445 **Figure 2.** a) Mean sound-speed profile derived from the deployment-average temperature and
 446 salinity, and used to compute b) the depth-correction term $\beta(h, f)$ following Cauchy et al.
 447 (2018). The correction accounts for the attenuation of wind-generated surface noise with
 448 increasing hydrophone depth and was applied prior to wind-speed retrieval. β is shown here
 449 for 3.15 kHz and 8 kHz.

Deleted: a) Sound speed profile used to derive the b) depth correction term $\beta(h, f)$ as a function of depth, following the formulation of Cauchy et al. (2018). The correction accounts for the attenuation of wind-generated surface noise with increasing sensor depth and was applied prior to wind speed estimation. Here, β is shown at 3.15 kHz and 8 kHz.

450 **2.4 Profiling float deployments**

Deleted:Page Break.....



460

461 **Figure 3.** Vertical profiles from the acoustic-equipped profiling float deployed near
 462 DYFAMED between February and April 2025. Blue points indicate times when passive
 463 acoustic data were successfully recorded. The vertical dashed line marks the transition between
 464 Deployment A and Deployment B.

465 Two deployments of an acoustic-equipped float (PROVOR CTS5) were carried out near
 466 DYFAMED between February and April 2025 (Fig. 1). Deployment A lasted 30 days, from 10
 467 February to 11 March, and Deployment B continued for 24 days starting on 12 March and
 468 remained active until 4 April. The float operated in park-and-profile mode at three parking
 469 depths (500, 700, and 1000 m; Fig. 2), collecting biogeochemical data during ascent and
 470 self-generated noise.

471 While Riser et al. (2008) previously demonstrated the feasibility of acoustic wind sensing from
 472 Argo floats, their system transmitted only pre-processed wind estimates derived onboard using
 473 a simplified version of the algorithm by Nystuen et al. (2015), without retaining or transmitting
 474 spectral band data. This limited the possibility of reanalysis or applying alternative processing
 475 schemes. In contrast, the floats used in this study recorded and transmitted full third-octave
 476 band spectra, enabling detailed post-processing and algorithm refinement tailored to the float's
 477 specific acoustic characteristics.

478 2.5 Transient and anthropogenic noise mitigation

479 Transient noise (i.e., episodic non-wind-related events) was mitigated by removing values
 480 exceeding the 99th percentile within a ± 1.5 -hour window centred around each matched
 481 timestamp. This percentile corresponds to discarding roughly the top 1% of samples over a 3-
 482 hour window (\approx two minutes of data). No physically meaningful wind- or wave-driven
 483 variability relevant to this study evolves on such short timescales, making this filter effective
 484 at removing brief acoustic artefacts without suppressing real high-wind conditions. This
 485 approach is conceptually similar to the transient-noise mitigation used in glider-based PAM
 486 studies (e.g., Cauchy et al., 2018), which suppress short-lived spikes in the spectra to isolate
 487 wind-generated noise.

Deleted: Transient noise (i.e. episodic non-wind-related events) was mitigated by removing values exceeding the 99th percentile within a ± 1.5 -hour window centred around each matched timestamp. While this approach risks excluding some high-wind events, we verified that extreme wind episodes typically span durations longer than a few hours, minimizing the chance of misclassification (see Fig. 8).⁴

496 To further reduce short-term variability and emphasize quasi-stationary wind-driven acoustic
 497 patterns, we applied a 3-hour rolling mean to each frequency band. This smoothing window is
 498 conceptually consistent with the profile-scale averaging used in glider-based acoustic wind
 499 studies (e.g., Cauchy et al., 2018), where acoustic measurements are aggregated over ~2-hour
 500 glider dives to suppress transient variability. While smoothing inevitably attenuates rapid
 501 fluctuations, the 3 h window stabilises the spectra without erasing multi-hour wind events
 502 relevant for air-sea flux applications. Alternative strategies, such as post-processing the wind
 503 speed estimates rather than the spectral bands, could be explored in future deployments if finer-
 504 scale variability is a priority.

505 Anthropogenic noise was mitigated using AIS vessel tracks. Because the float only provides
 506 GPS positions at the surface, we reconstructed a continuous trajectory by linearly interpolating
 507 its positions between successive surfacings at hourly resolution. Each 5-min acoustic record
 508 was then associated with the nearest interpolated position. An observation was flagged as
 509 potentially contaminated when an AIS-reported vessel was located within 20 km of this
 510 interpolated float position and within ± 30 min of the acoustic timestamp. The 20 km radius
 511 corresponds to the distance over which ship-radiated noise commonly dominates the ambient
 512 sound field in the 1–10 kHz band under low-to-moderate sea states, while the ± 30 min window
 513 accounts for the typically irregular AIS reporting interval offshore. As an additional safeguard,
 514 we excluded cases where the float-derived wind speed deviated from the DYFAMED buoy by
 515 more than the RMSE computed under uncontaminated conditions. This RMSE criterion is used
 516 only as a secondary check to capture possible contamination during periods of poor AIS
 517 coverage. Sensitivity tests indicate that moderate changes to these thresholds do not affect the
 518 main conclusions.

Formatted: Font: Times New Roman, 12 pt, Font color: Auto, English (UK)

Deleted: This choice reflects a compromise between noise reduction and temporal resolution: the smoothing is sufficient to stabilize wind estimates in the presence of submesoscale variability and intermittent noise, yet long enough to preserve multi-hour wind events of interest.

Deleted: this approach may attenuate

Deleted: very brief

Formatted: English (UK)

Deleted: , our inspection of the time series suggests that the smoothing is sufficient to suppress noise while retaining multi-hour processes of interest (eg., air-sea fluxes)

Formatted: Font: Times New Roman, 12 pt, Font color: Auto, English (UK)

Formatted: Justified

Deleted: To mitigate anthropogenic noise contamination, Automatic Identification System (AIS) ship tracking data were used to identify vessel presence within a 10 km radius and ± 30 minutes of each float timestamp. Acoustic observations were flagged as potentially contaminated if they coincided with ship presence and showed anomalous deviations—defined as float-derived wind speed differing from the DYFAMED buoy estimate by more than the root mean square error (RMSE) observed under uncontaminated conditions. While this introduces a partial dependence on external wind reference data, the combined AIS+anomaly criterion reduces false positives and avoids relying solely on model–sensor differences for data exclusion. Data flagged as contaminated were excluded from further analysis. [\[1\]](#)

543 **2.6 Application of established acoustic models**

Model	Input units	Wind frequency band (kHz)	Wind retrieval frequency (kHz)
Vagle et al. (1990)	dB re 1 $\mu\text{Pa}^2/\text{Hz}$	7.1–8.9	8
Nystuen et al. (2015)	dB re 1 $\mu\text{Pa}^2/\text{Hz}$	7.1–8.9	8
Pensieri et al. (2015)	dB re 1 $\mu\text{Pa}^2/\text{Hz}$	7.1–8.9	8
Cauchy et al. (2018)	dB re 1 μPa	2.8–3.55	3.15

544

← Formatted: Justified

545 **Table 2.** Summary of acoustic wind speed estimation models and their input requirements.
 546 Input units refer to the spectral level units used in model calibration. Central frequency
 547 indicates the nominal retrieval frequency, and the third-octave band column specifies the
 548 corresponding bandwidth. All models were calibrated and validated against standard 10-m
 549 wind speed.

550 Empirical models have long been used to estimate surface wind speed from underwater ambient
 551 noise, exploiting the link between wind-driven bubble formation and acoustic energy in the 1–
 552 20 kHz band. These models typically relate surface wind speed U to the sound pressure level
 553 L_f measured in selected frequency bands. While many models use third-octave bands, others
 554 rely on custom-defined or narrowband frequencies, often with variable bandwidths (e.g., 16%
 555 of the centre frequency in Vagle et al., 1990).

556 We applied four established wind retrieval models spanning a range of functional forms—
 557 cubic, two-regime linear–quadratic, composite, and two-regime log–linear. All wind models
 558 were applied using acoustic levels consistent with their original formulations (Table 2). This
 559 diversity allowed us to assess sensitivity to model structure and evaluate performance under
 560 float-specific conditions. Each model was first implemented using its published coefficients to
 561 generate wind speed estimates from float acoustic data, and the results were evaluated against
 562 collocated meteorological observations (Fig. 4). Subsequently, the parameters of each model
 563 were refitted using collocated float acoustic and wind data from the DYFAMED
 564 meteorological buoy (Figs. 4 and 5; see Table 1 in Supplementary Material), which provides
 565 hourly 10-meter wind speed. Model refitting was performed using nonlinear least-squares
 566 optimization (Table 3). Wind records from DYFAMED were matched to float measurements
 567 by nearest timestamp.

568 Following the spatial filtering approach of Cauchy et al. (2018), only float data within 40 km
 569 of DYFAMED were retained for refitting and validation (Fig. 1). This threshold corresponds
 570 to the estimated confidence radius around the DYFAMED meteorological buoy, within which
 571 wind speed measurements show high spatial coherence ($R = 0.86$, $\text{RMSE} = 2.5 \text{ m s}^{-1}$) when
 572 compared to the AROME-WMED atmospheric model (Rainaud et al., 2016). Although
 573 originally derived from the spatial wind-field decorrelation scale reported by Cauchy et al.
 574 (2018), this 40 km radius reflects a regional mesoscale atmospheric property rather than a
 575 platform-specific constraint. Because our deployment occurred in the same NW Mediterranean
 576 basin, this decorrelation length remains appropriate for our case. We note, however, that this
 577 threshold is region-dependent and should be re-evaluated for future deployments elsewhere.

Formatted: Not Superscript/ Subscript

Formatted: Font: Times New Roman, 12 pt, Font color: Auto, English (UK)

578 The updated coefficients were then used to generate wind estimates over the full float dataset.
 579 While this spatial proximity improves wind representativeness, it does not account for
 580 variations in wind fetch, a parameter known to influence ambient noise generation, particularly
 581 through wave and bubble field development (e.g., Prawirasrasa et al., 2024).

582 These four models were selected to represent a range of analytical formulations commonly
 583 used in acoustic wind retrievals. They all use frequency bands where wind-driven bubble noise
 584 typically dominates the local ambient sound field, with reduced interference from low-
 585 frequency sources such as distant shipping. Our aim was not to exhaust all available models,
 586 but rather to evaluate a representative subset under consistent float-specific conditions,
 587 emphasizing the effect of model structure and local fitting.

588 The specifications and key features of each model are summarized in Table 2 for reference.
 589 For all models and validation steps throughout the rest of Methods section, wind speed refers
 590 to the standard 10-meter wind speed, consistent with both the ERA5 reanalysis product and the
 591 DYFAMED buoy observations used for calibration and evaluation.

592 The first model, from Vagle et al. (1990), was derived from moored hydrophone data in the
 593 North Atlantic and relates wind speed to high-frequency noise at 8 kHz using a cubic
 594 formulation:

$$U_{\text{Vagle 1990}} = 10^{\frac{(-38.70 + \sqrt{-38.70^2 - 4.7 \cdot 38 \cdot (\text{SPL}_{8\text{kHz}} - 21.69)})}{-7.38 \cdot 2}} \quad (2).$$

Formatted: Justified

595 Next, we applied the cubic model from Nystuen et al. (2015), developed using long-term
 596 acoustic records from fixed hydrophones in both the Pacific and Atlantic. This model targets
 597 wind-generated noise at 8 kHz and includes band-specific criteria to distinguish wind
 598 contributions from other sources such as rain and shipping (Table 2).

$$U_{\text{Nystuen 2015}} = 0.0005 \cdot \text{SPL}_{8\text{kHz}}^3 - 0.0310 \cdot \text{SPL}_{8\text{kHz}}^2 + 0.4904 \cdot \text{SPL}_{8\text{kHz}} + 2.0871 \quad (3).$$

599 We then tested the two-regime linear–quadratic model from Pensieri et al. (2015) at 8 kHz,
 600 developed using moored hydrophone data from the Ligurian Sea, near our study area.
 601 Calibrated for Mediterranean conditions, the model relates wind speed to ambient noise levels
 602 at the 8 kHz band, applying distinct linear and quadratic fits across low- and high-noise
 603 regimes. Notably, the transition between regimes is defined at 38 dB, corresponding to a wind
 604 speed of 2.39 m s^{-1} in their framework. However, it is important to note that the threshold
 605 separating high and low regimes is not standardized across the literature and may vary between
 606 studies.

$$| \quad U_{\text{Pensieri 2015}} = \begin{cases} 0.044642 \cdot \text{SPL}_{8\text{kHz}}^2 - 3.2917 \cdot \text{SPL}_{8\text{kHz}} + 63.016 \\ 0.1458 \cdot \text{SPL}_{8\text{kHz}} - 3.146, \text{ for } \text{SPL}_{8\text{kHz}} < 38 \text{ dB} \end{cases} \quad (4).$$

Formatted: Justified

607 Finally, we included the two-regime log–linear model from Cauchy et al. (2018), developed
 608 using acoustic data from a glider operating in the western Mediterranean. Designed for mobile
 609 platforms, the model relates wind speed to third-octave noise levels centred at 3 kHz. The
 610 model uses distinct logarithmic and linear fits across two noise regimes.

611 This choice of 3 kHz, instead of the more commonly used 8 kHz, was based on empirical
 612 observations showing greater dynamic range and lower variance in this band, which may reflect
 613 sensor-specific factors or the sensor’s mounting configuration on the glider (Cauchy et al.,
 614 2018). The relationship goes as:

$$| \quad U_{\text{Cauchy 2018}} = \begin{cases} \frac{1}{0.4 \cdot 10^4} \cdot \left(10^{\frac{\text{SPL}_{3\text{kHz}} - S_{\text{off}}}{20}} + 0.2 \cdot 10^4 \right) \\ \frac{1}{1.6 \cdot 10^4} \cdot \left(10^{\frac{\text{SPL}_{3\text{kHz}} - S_{\text{off}}}{20}} + 12.5 \cdot 10^4 \right) \text{ for } U > 10 \text{ m s}^{-1} \end{cases} \quad (5).$$

Formatted: Justified

616 The wind retrieval relationship is modelled using a two-regime log-linear function. The
 617 transition between regimes occurs at wind speeds of approximately $10\text{--}11 \text{ m s}^{-1}$, established
 618 empirically. To represent this switching behaviour, a relative threshold level is introduced,
 619 expressed as $\text{SPL} - S_{\text{off}}$, where S_{off} denotes the sea-state 0 noise reference. This formulation
 620 highlights when wind-driven noise becomes dominant relative to the reference background
 621 noise.

622 2.7 Simulated wind estimation using reanalysis and residual learning

623 To assess the ability of float-derived acoustic measurements to estimate surface wind speed in
 624 regions lacking direct atmospheric observations, we developed a two-step framework based on
 625 (i) calibration to ERA5 reanalysis winds and (ii) residual correction using sparse in-situ
 626 measurements. The goal was to emulate realistic deployments of acoustic-equipped profiling
 627 floats in remote regions where only global reanalysis products and limited ship- or buoy-based
 628 wind measurements are available.

Formatted: Font: Times New Roman, 12 pt, Font color: Auto, English (UK)

Formatted: Normal, Space Before: 0 pt

Formatted: Font: Not Bold

629 **2.7.1 ERA5-based calibration of the acoustic model**

630 To evaluate the ability of float-derived acoustic measurements to estimate surface wind speed
 631 in regions lacking direct atmospheric observations, we used the ERA5 reanalysis from
 632 ECMWF (Bell et al., 2021). ERA5 provides global 10 m wind at 0.25° resolution and hourly
 633 frequency. We extracted zonal and meridional wind components (u_{10} , v_{10}) from the grid cell
 634 containing the float's position and computed wind speed U as:

$$U = \sqrt{u_{10}^2 + v_{10}^2} \quad (6).$$

635 These values were time-matched to float and DYFAMED measurements using the nearest
 636 available ERA5 hour.

637 The empirical acoustic–wind model of Nystuen et al. (2015; Eq. 3) was then re-fitted to the
 638 float's measured 8 kHz SPL using ERA5 wind speed as the reference. This produced an ERA5-
 639 calibrated acoustic wind estimate, representing a realistic scenario in which profiling floats
 640 operate in regions lacking direct wind observations and rely solely on reanalysis for model
 641 tuning.

642 Uncertainty in the ERA5-calibrated estimate was quantified using a 100-member bootstrap
 643 ensemble. For each iteration, we resampled the float dataset with replacement and perturbed
 644 the ERA5 wind input by adding Gaussian noise consistent with its reported uncertainty ($\sigma =$
 645 1.5 m s^{-1}). The acoustic model was re-fitted for each bootstrap sample, and the ensemble
 646 standard deviation was used to characterise uncertainty arising from both ERA5 input
 647 variability and the parameter sensitivity of the fitted empirical model.

648 **2.7.2 Residual -learning correction using limited in-situ observations**

649 To correct systematic errors in the ERA5-calibrated acoustic estimate, we used the limited
 650 DYFAMED buoy observations obtained within 40 km of the float. These collocated
 651 measurements represent approximately 40% of the full dataset and simulate practical scenarios
 652 in which only short-duration local reference winds (e.g., during deployment or opportunistic
 653 ship passages) are available.

654 Residuals between DYFAMED wind speed and the ERA5-calibrated acoustic estimate were
 655 modelled using four predictors: SPL at 8 kHz, ERA5 10-m wind speed, normalised deployment
 656 day, and the Nystuen-model wind estimate. These variables capture the local acoustic signal,
 657 large-scale atmospheric forcing, slow temporal drift, and the first-order empirical fit. Residuals
 658 were estimated with XGBoost regression (Chen & Guestrin, 2016), using all float-buoy
 659 collocations within 40 km (~40% of the dataset). To maintain generalisation, we applied a
 660 compact hyperparameter set (300 estimators, learning rate 0.05, max depth 3, subsample 0.9,
 661 colsample bytree 0.8) together with safeguards against overfitting, including bootstrap
 662 resampling, Gaussian perturbations of ERA5 winds ($\sigma = 1.5 \text{ m s}^{-1}$) during training and
 663 prediction, shallow trees, and subsampling of both rows and features. Uncertainty was
 664 quantified using a 100-member ensemble, with each model trained on a bootstrap resample of

Formatted: Font: (Default) Times New Roman, 12 pt, **Bold**

Formatted: Font: (Default) Times New Roman, 12 pt, **Bold**,
Font color: Auto, English (UK)

Formatted: Subscript

Formatted: Subscript

Deleted: To evaluate the ability of float-derived acoustic measurements to estimate surface wind speed in regions without direct atmospheric observations, we used wind data from the ERA5 atmospheric reanalysis produced by the European Centre for Medium-Range Weather Forecasts (ECMWF; Bell et al., 2021). ERA5 provides global wind fields on a $0.25^\circ \times 0.25^\circ$ spatial grid with hourly temporal resolution, offering a consistent and widely used reference for surface atmospheric conditions.[¶]

Hourly ERA5 data were retrieved for the period spanning the float deployments, from 10 February to 31 March 2025. Specifically, we extracted the 10 m zonal (u_{10}^2) and meridional (v_{10}^2) wind components from the grid cell containing the float's position. Wind speed (U) was then computed as:

Formatted: Justified

Formatted: Font: Times New Roman, 12 pt, Font color: Auto, English (UK)

Formatted: Font: Times New Roman, 12 pt, Font color: Auto, English (UK)

Deleted: Using ERA5 wind speeds as a reference, we refitted the empirical model from Nystuen et al. (2015; 3) to float-measured Sound Pressure Level (SPL) at 8 kHz, producing a new set of coefficients tailored to the float deployment. This produced a first-pass wind estimate derived from float acoustics alone, calibrated to ERA5 rather than to DYFAMED in-situ observations. This approach simulates a scenario in which a profiling float is deployed in a remote region lacking surface wind measurements, and reanalysis products are used to train or tune the acoustic model.[¶]

Formatted: Font: Times New Roman, 12 pt, Font color: Auto, English (UK)

Formatted: Justified

Formatted: Font: (Default) Times New Roman, 12 pt, **Bold**,
Font color: Auto, English (UK)

Formatted: Heading 1, Justified, Space Before: 24 pt

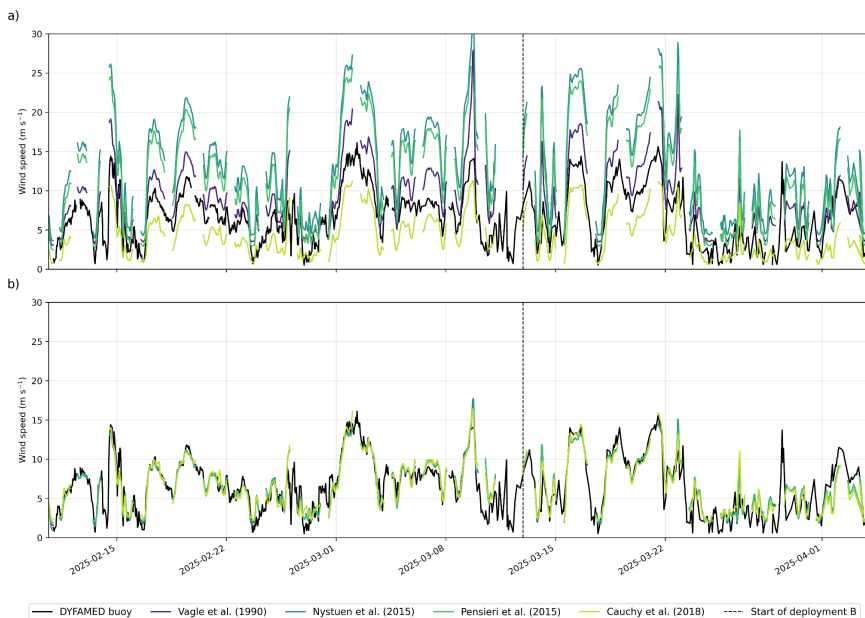
Formatted: Font: Times New Roman, 12 pt, Font color: Auto, English (UK)

Formatted: Font: (Default) Times New Roman, 12 pt, Font color: Auto, English (UK)

Formatted: Space Before: 0 pt, After: 0 pt

691 the DYFAMED-matched subset and forced with perturbed ERA5 winds. This dual
 692 bootstrapping captures variability associated with the machine learning model structure and
 693 with ERA5 uncertainty. Corrected wind speeds were obtained by adding the ensemble-mean
 694 residual to the ensemble-mean Nystuen estimate, with total uncertainty expressed as $\pm 1\sigma$ by
 695 combining the XGBoost ensemble spread and ERA5 input uncertainty in quadrature. The
 696 bootstrap uncertainty of the Nystuen fit is reported separately. This framework provides a
 697 transparent and robust correction method, illustrating how float acoustics, reanalysis winds,
 698 and sparse in-situ observations can be combined to estimate surface wind speed in remote
 699 regions.

700 3 Results and Discussion



701

702 **Figure 4.** Comparison of unoptimized (top) and optimised (bottom) wind speed models against
 703 DYFAMED buoy observations. Each subplot shows modelled wind speed estimates from four
 704 literature models (Vagle et al., 1990; Nystuen et al., 2015; Pensieri et al., 2015; Cauchy et al.,
 705 2018) compared with collocated buoy wind data (black line). The unoptimized models a) use
 706 original published coefficients, while the optimised models b) are re-fitted using data within
 707 40 km of the DYFAMED site. The dashed vertical line indicates the start of deployment B.

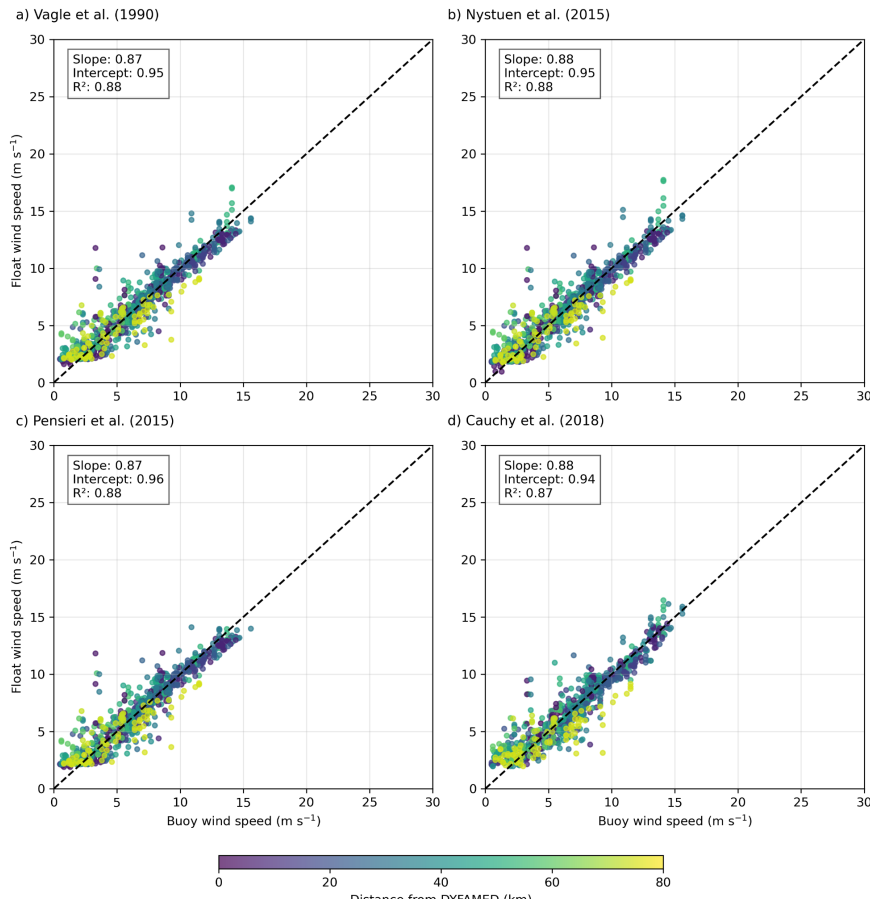
Formatted: Font: (Default) Times New Roman, 12 pt, Font color: Auto, English (UK)

Deleted: To improve the accuracy of this ERA5-calibrated estimate, we developed a residual learning framework that uses limited collocated DYFAMED in-situ observations to correct systematic errors. This training set, consisting of observations within 40 km, represents approximately 40% of the full dataset. This setup was designed to simulate a realistic scenario where ship-based wind measurements are available in proximity to a float deployment. Specifically, we used wind speed measurements from the DYFAMED buoy to model residual differences between the ERA5-based acoustic prediction and true surface conditions. A feature matrix was constructed including SPL at 8 kHz, ERA5 wind speed (10-meter), normalized time (deployment day), and the acoustic model prediction wind speed from Nystuen et al. (2015; Eq. 3). Residuals relative to DYFAMED wind speed were modelled using XGBoost regression, gradient-boosting machine learning algorithm based on gradient-boosted decision trees and known for its high predictive performance and ability to handle non-linear relationships and interactions between features (Chen and Guestrin, 2016).

Deleted: To estimate prediction uncertainty, we applied bootstrapping at two levels. For the ERA5-calibrated acoustic estimate, we generated 100 bootstrap samples by resampling the float dataset with replacement and perturbing the ERA5 wind input using its reported uncertainty (standard deviation $\sigma = 1.5 \text{ m s}^{-1}$; Bell et al., 2021). The empirical model was re-fitted for each bootstrap, and the resulting ensemble of predictions was used to compute the standard deviation at each time point. This approach captures both the impact of ERA5 input uncertainty and variability in the fitted model parameters.

For the ML-corrected wind speed, we trained an ensemble of 100 XGBoost models on bootstrapped subsets of the training data. During both training and prediction, Gaussian noise ($\text{mean} = 0, \sigma = 1.5 \text{ m s}^{-1}$) was added to the ERA5 wind feature to simulate observational uncertainty. The Gaussian assumption provides a tractable way to propagate uncertainty through the learning framework and is commonly used in ensemble perturbation methods when only first- and second-moment statistics are available. While the true distribution of ERA5 errors may deviate from normality, the central limit tendency of aggregated atmospheric errors makes the Gaussian approximation a reasonable first-order choice. Importantly, this approach ensures that the output uncertainty reflects both the variability of the fitted ML model and the stated input uncertainty, though future work could refine the noise model if detailed error distributions become available. Final corrected wind speeds were computed by summing the Nystuen et al. (2015) ensemble-mean prediction with the ensemble-mean residual. Uncertainty bounds were defined as $\pm 1\sigma$, combining variability across the XGBoost ensemble with ERA5 input uncertainty in quadrature. Uncertainty for the ML-corrected estimate reflects the variability of the residual model and ERA5 input uncertainty but does not propagate the bootstrap spread of the underlying Nystuen fit, which we report separately.

This method demonstrates how passive acoustic observations from profiling floats can be combined with global reanalysis products and limited in-situ data to improve local wind speed estimates, simulating the upscaling of BGC-Argo float deployments in remote ocean regions lacking direct v... [14]



815

816 **Figure 5.** Comparison of optimised wind speed estimates from four literature models against
 817 collocated DYFAMED buoy wind measurements. Each subplot (a–d) shows scatter plots of
 818 float-derived wind speed vs. buoy wind speed using model-specific optimised coefficients: (a)
 819 Vagle et al. (1990), (b) Nystuen et al. (2015), (c) Pensieri et al. (2015), and (d) Cauchy et al.
 820 (2018). Points are color-coded by distance from the DYFAMED buoy, and the dashed line
 821 represents the 1:1 reference. Insets display linear regression slope, intercept, and coefficient of
 822 determination (R^2).

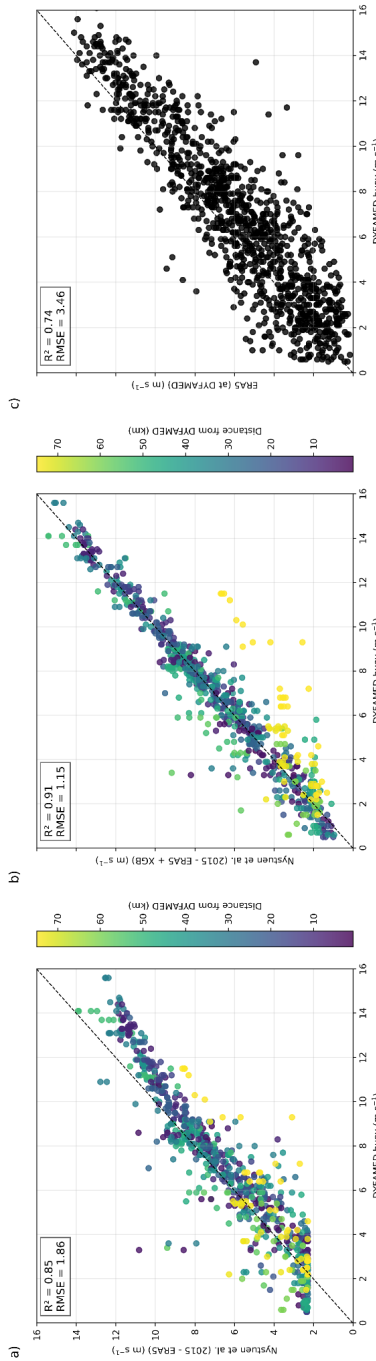
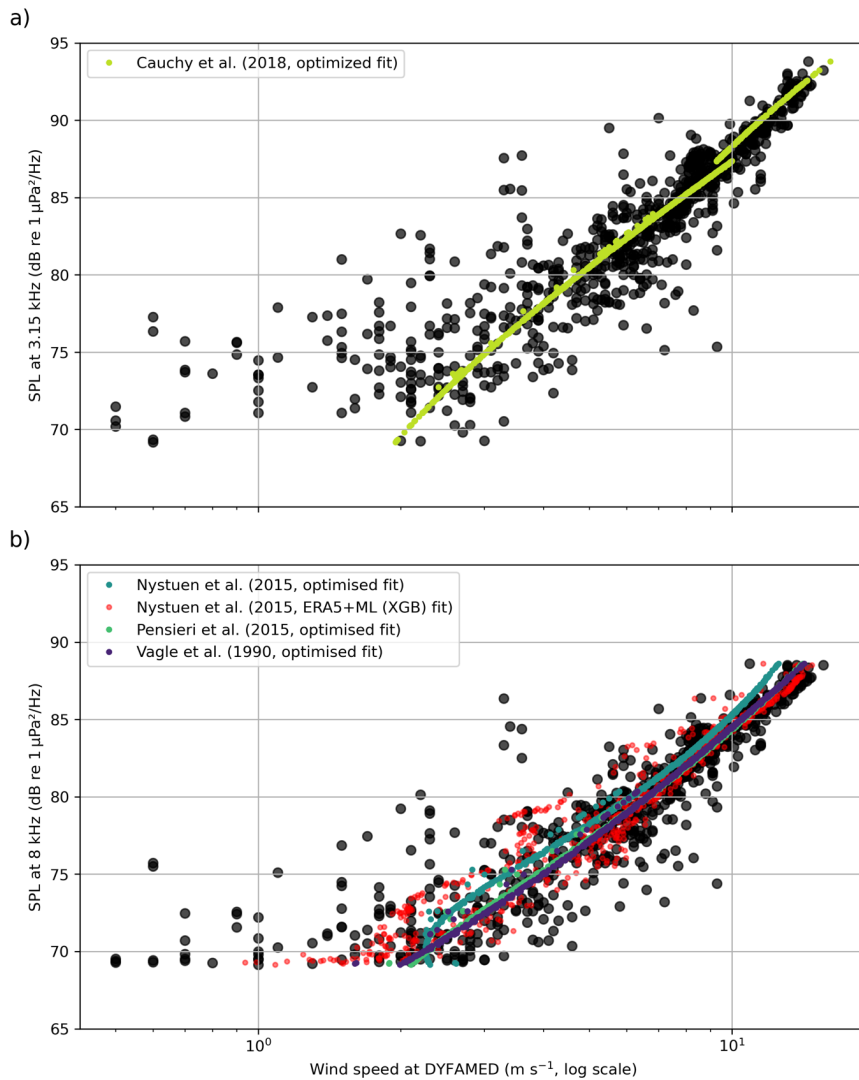
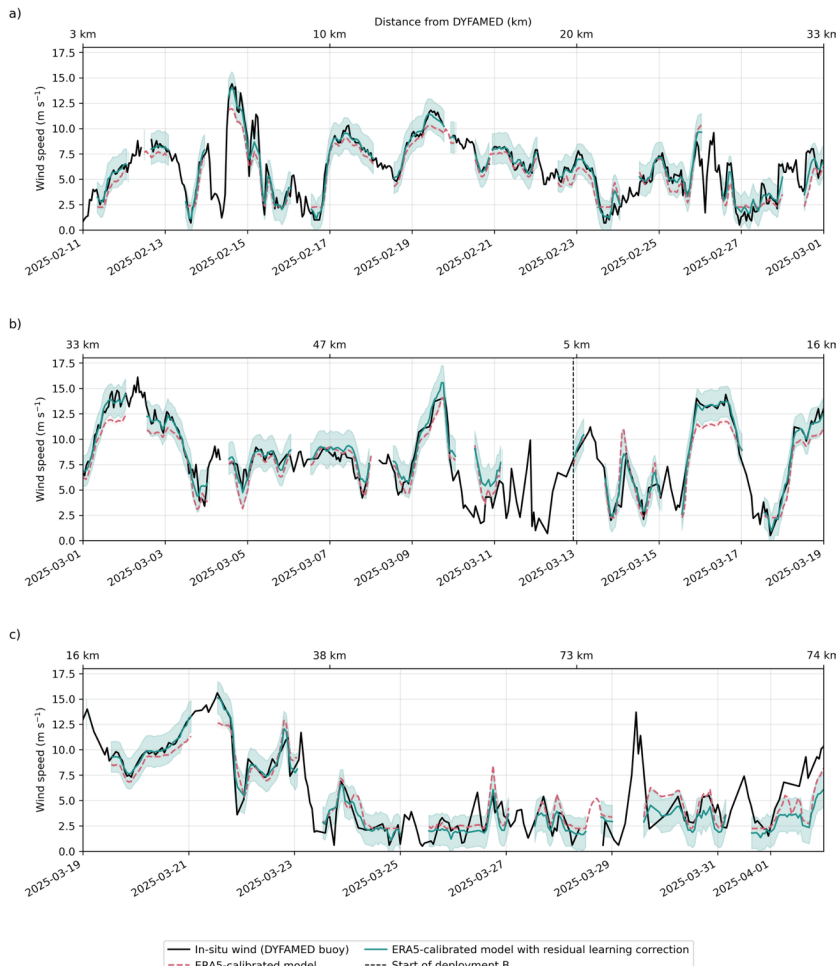


Figure 6. Comparison between DYFAMED buoy wind speed measurements and float-derived estimates using the Nystuen et al. (2015) acoustic model: (a) wind speeds estimated using Nystuen's polynomial formulation fit to ERA5; (b) same model corrected using a residual-learning approach with XGBoost, trained on the differences between ERA5-based estimates and DYFAMED observations; and (c) ERA5 wind speed at the DYFAMED grid point compared directly to buoy measurements for February, March and April 2025. Each point is colored by the float's distance from DYFAMED in panels (a) and (b). Dashed lines denote 1:1 agreement. All wind speeds are expressed in meters per second (m s⁻¹).



826 **Figure 7.** Optimised 10-meter wind speed (log scale) as a function of observed underwater
 827 sound pressure level (SPL) at DYFAMED for (a) 3.15 kHz and (b) 8 kHz. Observed wind speed
 828 is shown in black.



830

831 **Figure 8.** Time series comparison between acoustic float wind estimates and DYFAMED buoy
 832 winds, displayed over three consecutive 18-day windows (a–c). The dashed pink curve
 833 corresponds to wind speeds predicted using the Nystuen et al. (2015) acoustic model calibrated
 834 solely with ERA5 reanalysis winds. The solid green curve shows the same model after applying
 835 the residual-learning correction (XGBoost), and the shaded region indicates its associated
 836 predictive uncertainty. Buoy-measured wind speed is shown in black. The upper x-axis reports
 837 the float's distance from DYFAMED throughout the record, and the dashed vertical line
 838 indicates the transition to deployment B.

839

Deleted: Time series comparison of wind speed estimates from the acoustic float and DYFAMED buoy observations, shown across three sequential 18-day segments of the deployment (a–c). The dashed pink line shows estimates from the Nystuen et al. (2015) model fit to ERA5-derived inputs. The solid green line represents the same model corrected using a residual-learning approach (XGBoost) with its associated uncertainty. Black curves show in-situ wind speed from the DYFAMED buoy. The top x-axis indicates the float's distance from DYFAMED over time, and a dashed vertical line marks the start of deployment B.

851 **3.1 Assessing the performance of float-based acoustic wind estimation**

852 We applied four previously published wind retrieval models to float-measured sound pressure
 853 levels (SPLs) at 8 kHz and 3 kHz. Using the original coefficients from these studies, wind speed
 854 estimates deviated significantly from collocated DYFAMED observations, particularly in their
 855 ability to reproduce the magnitude of wind events (Fig. 4a). This mismatch reflects the
 856 sensitivity of empirical acoustic models to deployment context, including platform geometry,
 857 acoustic propagation, and local noise environment.

858 When these same models were refitted using collocated float acoustics and DYFAMED wind
 859 observations within 40 km (Fig. 1), performance improved substantially (Fig. 4b; Fig. 7).
 860 Among the models, the cubic formulation by Nystuen et al. (2015) achieved the best fit
 861 ($R^2 = 0.88$; Fig. 5b) and successfully captured the full observed wind range (0.5–16.1 m s⁻¹;
 862 Figs. 5 and 7). It was also the only model resolving wind speeds ≤ 2 m s⁻¹, a regime often missed
 863 due to weak surface forcing and minimal bubble generation. This low-wind sensitivity
 864 strengthens its relevance for air-sea gas-exchange studies and suggests broad applicability in
 865 moderate wind regimes. High-quality wind estimates are particularly important for interpreting
 866 float-based biogeochemical measurements, as air-sea oxygen fluxes respond sensitively to
 867 short-timescale wind variability (Bushinsky et al., 2017).

868 However, even after successful fitting, the portability of acoustic-wind models remains
 869 uncertain. Factors such as noise contamination, ambient biological activity and regional
 870 propagation conditions can vary substantially between deployments, affecting both the shape
 871 and robustness of the acoustic-wind relationship (Gros-Martial et al., 2025b). Moreover,
 872 profiling floats introduce their own artifacts, which may arise from hydrodynamic turbulence,
 873 buoyancy engine activity, bubble release, or electronic interference, each of which can
 874 contaminate the acoustic signal independently of wind forcing. Even models developed in the
 875 same basin required refitting (i.e. Pensieri et al. 2015; Figs. 4, 5 and 7).

876 A promising direction would be to classify deployments into broader “acoustic environment
 877 types”, such as open-ocean gyres, coastal shelves, or high-latitude storm zones, within which
 878 shared model parameters could be defined and validated. This aligns with the priorities outlined
 879 in the Ocean Sound Essential Ocean Variable (EOV) Implementation Plan, which emphasizes
 880 the need for community-agreed metadata standards, calibration protocols, and classification
 881 schemes to support global comparability across acoustic deployments (Tyack et al., 2023).
 882 Evaluating these frameworks for profiling floats may help standardize acoustic wind retrieval
 883 and integrate it more effectively into global observing systems.

884 **3.2 Generalizing float-specific wind modelling using reanalysis**

885 While site-specific fitting of acoustic wind models yields accurate float-derived wind
 886 estimates, such fittings are not feasible in most regions of the global ocean where in-situ wind
 887 observations are unavailable. To assess whether the acoustic-wind relationship can be
 888 generalized for remote deployments, we investigated the use of reanalysis wind products as a
 889 proxy reference for model fitting. Specifically, we used the ERA5 atmospheric reanalysis (Bell
 890 et al., 2021) to refit the Nystuen et al. (2015) model to float-measured acoustic data, simulating
 891 a scenario where no collocated buoy or shipboard wind measurements are available (Figs. 6
 892 and 8).

Deleted: markedly

Deleted: Notably

Deleted: ,

Deleted: i

Deleted: capable of

Deleted: below

Deleted: a critical range often

Deleted: underrepresented

Deleted:

Formatted: Default Paragraph Font, Font color: Auto, English (UK)

Formatted: Font: Times New Roman, 12 pt, Font color: Auto, English (UK)

Deleted: This low-end sensitivity is particularly valuable for air-sea gas exchange estimates in biogeochemical studies and suggests that the Nystuen model may be more broadly applicable in low-to-moderate wind regimes.

Deleted: transferability

Deleted: . In our study,

Deleted: e

Deleted: originally

Deleted: , underlini

Deleted: ng the challenge of cross-platform and cross-region generalization.

Deleted: future

Deleted: may involve

Deleted: grouping

Deleted: —

Deleted: —

Formatted: Default Paragraph Font, Font color: Auto, English (UK)

Deleted: Evaluating the adequacy of such frameworks in the context of profiling float-based wind retrieval could inform future updates and promote harmonization with broader ocean observing efforts.

Deleted: ¶

923 Using time-matched float sound pressure level at 8 kHz and collocated ERA5 wind speed, we
 924 derived a new set of coefficients (Section 2.6), ~~producing a general-purpose fit based solely on~~
 925 ~~float data and reanalysis inputs. The goal was to test whether an existing model can be adapted~~
 926 ~~for use in data-sparse regions, enabling scalable wind estimation from profiling floats.~~

927 As shown in Figure 6a, the ERA5-calibrated Nystuen et al. (2015) model reproduced wind
 928 variability within the 2.5–10 m s⁻¹ range with moderate skill ($R^2 = 0.85$), and performed best
 929 during Deployment A, when wind conditions remained relatively stable (Fig. 8). ~~Performance~~
 930 ~~deteriorated during stronger wind events, particularly in Deployment B, where the model~~
 931 ~~systematically underestimated wind, with errors > 3 m s⁻¹ (Figs. 6a and 8).~~

932 Comparison with DYFAMED also revealed broader limitations of ERA5. Although ERA5
 933 provides a globally consistent wind product, it diverged from buoy observations during several
 934 high-wind episodes. This behaviour is consistent with earlier reports of reanalysis
 935 underestimating localised, orographically forced winds in semi-enclosed basins such as the
 936 Mediterranean (Bentamy et al., 2003; Bell et al., 2021). Such biases are critical in regions like
 937 the Southern Ocean, where frequent high-wind events dominate air-sea CO₂ fluxes and gas
 938 exchange scales nonlinearly with wind speed (Wanninkhof, 2014; Wanninkhof et al., 2025).

939 ~~Thus, while float reanalysis-based calibration enables acoustic wind estimation in the absence~~
 940 ~~of local observations, its accuracy depends strongly on the reliability of the reference product~~
 941 ~~used for fitting.~~

942 3.3 Simulating scalable wind estimation in data-sparse regions

943 While reanalysis-calibrated acoustic models offer a pathway for estimating surface wind speed
 944 in remote regions, the results in Section 3.2 show that this approach alone is insufficient during
 945 high-wind or rapidly evolving events. ~~This limitation is especially critical in high-latitude~~
 946 ~~regions such as the Southern Ocean, where extreme wind forcing drives critical fluxes of heat,~~
 947 ~~momentum, and carbon (Gray et al., 2018; Dotto et al., 2019; Zhang et al., 2022; Gruber et al.,~~
 948 ~~2023).~~

949 3.3.1 Local model correction using residuals learning

950 To overcome this, we implemented a residual learning framework that combines the
 951 generalizability of reanalysis-based fitting with the accuracy of localized corrections.
 952 Specifically, we trained an ensemble of XGBoost regression models to predict the residuals
 953 between the ERA5-calibrated estimates and collocated DYFAMED buoy observations (see
 954 Section 2.6). The model was trained using float data within 40 km of DYFAMED and
 955 bootstrapped over 100 iterations to quantify mean corrections and prediction uncertainty (Fig.
 956 1; Fig. 6b). The 40 km radius was selected based on the sensitivity analysis of Cauchy et al.
 957 (2018), who found it to balance proximity with data availability; ~~though this threshold is likely~~
 958 ~~site-dependent and should be reassessed in future deployments.~~

959 The corrected wind time series showed substantially better agreement with DYFAMED
 960 observations (Fig. 8), especially during high-wind events where the uncorrected model
 961 underestimated wind speeds. This bias correction increased R^2 from 0.85 to 0.91 and reduced
 962 RMSE from 1.88 m s⁻¹ to 1.15 m s⁻¹, a 37.0% reduction in prediction error. While other

Deleted: representing

Formatted

... [15]

Deleted: a general-purpose acoustic wind model that could, in principle, be deployed globally using only float data and reanalysis inputs. The objective of this exercise was not to develop a new region-specific model, but rather to test whether existing models could be adapted—via reanalysis fitting—for use in data-sparse areas, ultimately enabling scalable wind estimation from profiling floats globally.

Deleted: is

Deleted: -1

Deleted: $R^2 = 0.85$, and performed best during Deployment A, when wind conditions remained relatively stable and within the moderate wind regime ... Fig. 8). However..., ~~Performance~~ declined ... deteriorated during periods of stronger wind... during stronger wind events, particularly in Deployment B (Figs. 6a and 8)... where the. In these cases, the ... model systematically underestimated wind speeds... with errors > exceeding

... [16]

Formatted: Superscript

Formatted: Superscript

Deleted: during high-wind events.

Formatted: Not Superscript/ Subscript

Deleted: ERA5 reanalysis... YFAMED also revealed broader limitations of ERA5. Although ERA5 provides a globally consistent wind product, reference product for surface winds... it diverged from DYFAMED ... buoy observations data ... using several high-wind episodes, especially in Deployment B... This discrepancy ... behaviour is consistent with earlier studies ... reports reporting the underestimation of localized orographic wind events in

... [17]

Formatted

... [18]

Deleted: reanalysis datasets over semi-enclosed basins such as the Mediterranean

Formatted: Subscript

Deleted: This limitation is especially consequential for deployments in the Southern Ocean, where high-wind...

... [19]

Deleted: Thus, while float-based acoustic wind estimation can be extended using reanalysis data in the absence

... [20]

Formatted: Justified

Formatted

... [21]

Deleted: alone remains insufficient during high-wind events or rapidly evolving conditions.

Formatted

... [22]

Deleted: This limitation poses a significant challenge for air-sea interaction studies in the Southern Ocean and

... [23]

Deleted: Lee et al., 2017;

Formatted: Font: Times New Roman, 12 pt, Font color: Auto, English (UK)

Deleted: to estimate both mean corrections and predictive uncertainty ... Fig. 1; Fig. 6b). The 40 km radius was

... [24]

Deleted: markedly ... substantially improved ... after alignment ... agreement with DYFAMED observations

... [25]

1166 learning-based methods have achieved similar improvements (e.g., ; Zambra et al., 2023, 16%
 1167 RMSE reduction), our method explicitly uses reanalysis as a prior and relies only on sparse in-
 1168 situ fitting, making it more realistic for remote deployments.

1169 The machine learning model does not estimate wind speed directly, but instead learns to adjust
 1170 biases using a small set of predictors, (i.e.: acoustic signal intensity, deployment day, ERA5-
 1171 calibrated prediction). In effect, it identifies conditions under which ERA5 is likely to fail,
 1172 applying larger corrections during high-wind events.

1173 These results demonstrate that even limited in-situ reference data—for example, brief engine-
 1174 off ship-based winds during deployment—can significantly improve estimates along the full
 1175 float trajectory. In our case, in-situ points represented approximately 40% of the record due to
 1176 the short deployment but this introduces potential limitations. First, because fitting and
 1177 evaluation used the same dataset, the performance metrics may be optimistic. Future
 1178 deployments should use spatially or temporally separate validation or fully independent
 1179 reference stations. Second, the RMSE reduction reflects improvements mainly at high wind
 1180 speeds, where raw errors are largest, and may overstate gains at lower winds. Taken together,
 1181 these factors imply that these performance metrics likely represent an upper bound of the
 1182 framework’s accuracy for long-duration or multi-region deployments. The generalisation
 1183 across sites, seasons and events remains untested and will require validation using spatially or
 1184 temporally independent datasets.

1185 3.3.2 Strategies for sparse in-situ calibration

1186 In practical terms, acquiring suitable reference observations can be challenging. While ship-
 1187 based wind measurements are a natural candidate, particularly during float deployment or
 1188 recovery, they may be unsuitable for model fitting if the ship is too close, as engine noise can
 1189 contaminate the float’s acoustic signal. A practical compromise is to station the ship far enough
 1190 to avoid acoustic interference while keeping wind measurements representative. Alternatively,
 1191 a more robust strategy is to deploy floats in proximity to existing meteorological buoys, which
 1192 provide collocated wind observations without interfering with subsurface acoustic recordings.

1193 In regions where neither buoys nor suitable ship data are available, identifying whether the
 1194 available in-situ coverage is sufficient becomes more complex. This will depend not only on
 1195 the duration and trajectory of the float mission, but also on the opportunistic use of additional
 1196 reference sources encountered along the way, for example, other buoys, or wind observations
 1197 from vessels transiting the area. Where such sources are absent, satellite products, particularly
 1198 synthetic aperture radar (SAR), can provide episodic but high-resolution wind fields that
 1199 capture localized variability and serve as intermittent calibration points.

1200 More broadly, these scenarios highlight the need for flexible modelling approaches that can
 1201 exploit heterogeneous and temporally limited reference data. Rather than relying on dense
 1202 training datasets or persistent surface observations, future efforts could employ machine-
 1203 learning strategies such as domain adaptation, transfer learning, or few-shot learning to adapt
 1204 models to new environments with minimal retraining. For instance, recent work by Wang et al.
 1205 (2020) has shown that few-shot transfer methods can yield competitive performance even when
 1206 only a small number of target-domain samples are available.

Deleted: comparable

Deleted: —

Deleted:) reported a 16% RMSE reduction using a physics-informed deep learning model—our method differs by explicitly using reanalysis as a prior and requiring only sparse in-situ fitting.

Deleted: . I

Deleted: , it

Deleted: the bias

Deleted: based

Deleted: on

Deleted: limited

Deleted: number

Deleted: input features

Deleted: :

Deleted: and the

Deleted: In essence, it identifies when and where ERA5 is likely to fail, applying larger corrections under high-wind conditions where reanalysis tends to underestimate variability.

Deleted: a

Formatted: Default Paragraph Font, Font color: Auto, English (UK)

Formatted: Font: Times New Roman, 12 pt, Font color: Auto, English (UK)

Deleted: limited number of in-situ fitting points—simulating, for example, a brief engine-off ship-based wind measurement window during float deployment—cou[... [26]

Deleted: the

Deleted: data

Deleted: used for fitting

Deleted: of the full dataset,

Deleted: relatively

Deleted: duration. However,

Deleted: this approach also introduces potential limitations.

Formatted

[27]

Deleted: although we aimed to simulate operational

[30]

Formatted

[28]

Formatted

[29]

Deleted: however,

Deleted: —

Deleted: —

Deleted: A viable compromise is to position the ship [... [31]

Deleted: —

Deleted: In such cases, satellite-based products—

[32]

Deleted: future efforts could explore machine learnin[... [33]

1278 In the context of profiling floats, such strategies could enable a more scalable approach to
 1279 acoustic model tuning, leveraging sparse data from ships, buoys, or satellites, each limited
 1280 individually but collectively offering adequate diversity. We propose framing this
 1281 as opportunistic multisource model fine-tuning: a hybrid calibration scheme in which local
 1282 corrections are derived from whatever reference sources are available, without requiring dense
 1283 or continuous in-situ coverage. Developing and validating such approaches will be essential
 1284 for global deployment of acoustically equipped floats while maintaining robustness across
 1285 diverse environmental and acoustic conditions.

1286 3.3.3 Implications for global observing

1287 While ERA5 provides a useful climatological reference, it tends to underestimate short-lived,
 1288 high-wind events due to spatial and temporal smoothing (Fig. 8). This is an issue particularly
 1289 for gas exchange studies, as extreme winds disproportionately contribute to total fluxes.
 1290 Acoustic float data, collected continuously and at high resolution, offer the potential to
 1291 complement satellite or reanalysis wind products, particularly during short-lived wind events
 1292 that are smoothed out in coarse-resolution products.

1293 However, model performance degrades with increasing distance from DYFAMED, reflecting
 1294 the spatial decorrelation of wind fields and the limited spatial representativeness of the buoy
 1295 observations. Beyond 73 km during Deployment B, both the Nystuen et al. (2015) – ERA5 fit
 1296 and the machine-learning-corrected float estimates begin to diverge from DYFAMED winds
 1297 (Figs. 6 and Fig. 8). This divergence likely reflects true spatial variability rather than model
 1298 failure, as the float and buoy may be sampling different wind regimes. One way to address this
 1299 uncertainty is to analyse float trajectories that pass between two surface reference stations,
 1300 testing whether refitting at the final station yields consistent corrections or reveals systematic
 1301 regional shifts in wind decorrelation. Such an approach will require future deployments that
 1302 span multiple buoys, enabling a systematic evaluation of how model performance degrades, or
 1303 remains robust, across both time and space.

1304 Additionally, in the Southern Ocean, where anthropogenic noise is relatively low, lower-
 1305 frequency bands (<1 kHz) may be viable for wind estimation, as they are more sensitive to high
 1306 wind speeds due to increased bubble activity and longer propagation ranges. These bands could
 1307 outperform higher-frequency bands under strong forcing conditions, provided contamination
 1308 from distant shipping or other sources remains minimal.

1309 Several recent studies have applied machine learning to underwater acoustic data to estimate
 1310 wind and rainfall, often relying on long-term, stationary deployments and direct spectral
 1311 prediction (Taylor et al., 2020; Trucco et al., 2022; Trucco et al., 2023; ; Zambra et al., 2023).
 1312 While effective under controlled conditions, these approaches depend on dense labelled
 1313 datasets and assume stable acoustic environments. In contrast, our residual-learning strategy is
 1314 designed for sparse, mobile deployments: it corrects reanalysis-based estimates using short-
 1315 duration in-situ fitting and does not require full acoustic labels, making it more compatible with
 1316 the operational realities of profiling floats.

1317 While in-situ data remains the most difficult to obtain in remote regions, our method supports
 1318 opportunistic fitting, for example, brief ship-based winds during deployment or nearby
 1319 meteorological buoys. This hybrid strategy balances scalability and realism, enabling more
 1320 robust performance even where long-term reference data are scarce.

Formatted: Justified, Space Before: 12 pt, After: 12 pt

Formatted: Default Paragraph Font, Font color: Auto, English (UK)

Deleted: by leveraging sparse data from ships, buoys, or satellites—each with its own limitations but collectively offering sufficient diversity

Formatted: Font: Times New Roman, 12 pt, Font color: Auto, English (UK)

Formatted: Default Paragraph Font, Font color: Auto, English (UK)

Formatted: Font: Times New Roman, 12 pt, Font color: Auto, English (UK)

Formatted: Default Paragraph Font, Font color: Auto, English (UK)

Deleted: We propose framing this as opportunistic multisource model fine-tuning: a hybrid calibration scheme in which local corrections are derived from whatever reference sources are available, without requiring dense or continuous in-situ coverage. Developing and validating such methods will be essential to deploy acoustic-equipped floats globally while maintaining robustness across a wide range of environmental and acoustic conditions.
 Page Break

Deleted: Acoustic float data—collected continuously and at high resolution—are uniquely positioned to detect these events, even when they fall below the detection threshold of satellite or reanalysis products.

Deleted: This divergence does not necessarily imply model failure but rather raises the possibility that the float and buoy are sampling different wind regimes. In such cases, it becomes difficult to determine whether discrepancies are due to limitations in the acoustic model or to true spatial variability in wind forcing

Deleted: assessing whether refitting at the final station yields consistent corrections or reveals systematic regional shifts in wind decorrelation

Deleted: —

Deleted: —

Deleted: it may also be worth reconsidering the use of lower-frequency bands (<1 kHz) for wind estimation. ... [34]

Deleted: and may

Deleted: —

Deleted: from spectral features

Deleted: While these approaches have shown strong performance under controlled conditions—such as T... [35]

Formatted: Font: Times New Roman, 12 pt, Font color: Auto, English (UK)

Formatted: Default Paragraph Font, Font color: Auto, English (UK)

Deleted: In contrast, our residual learning strategy is designed for sparse, mobile deployments. It corrects ... [36]

Deleted: , data-poor

Deleted: our approach is well-suited to opportunistic fitting—for instance, using brief ship-based wind ... [37]

1382 Another important consideration is the potential for regional bias introduced by the depth
1383 correction applied to acoustic levels. This correction compensates ~~driven by local hydrographic~~
1384 ~~structure and was derived from the float's mean profile at the start of the deployment. Applying~~
1385 ~~a single correction to the full mission introduces a location-dependent bias that may vary across~~
1386 ~~floats or seasons. Ideally, the correction should be recalculated with each new hydrographic~~
1387 ~~profile, especially for long-term or wide-ranging deployments. To ensure basin-to global-scale~~
1388 ~~comparability, these corrections should be standardised and explicitly documented in~~
1389 ~~processing protocols for acoustic-equipped floats.~~

1390 This deployment-focused flexibility is key to scaling up acoustic wind estimation globally. ~~By~~
1391 ~~combining reanalysis for first-order fitting with localized corrections when available, our~~
1392 ~~framework improves agreement with in-situ winds without requiring long-term surface~~
1393 ~~infrastructure. Scaling this approach across the BGC-Argo array would provide high-~~
1394 ~~resolution, all-weather wind monitoring in regions poorly served by existing observing~~
1395 ~~networks.~~

Deleted: In parallel,

Deleted: a

Deleted: f

Deleted: or propagation losses due to local water column properties (e.g., temperature, salinity, and sound speed) and i

Deleted: s

Deleted: typically

Deleted: hydrographic

Deleted: When used to adjust the full acoustic time series, this introduces a location-dependent correction that may vary across floats or missions.

Deleted: for

Deleted: in

Deleted: where temperature and salinity conditions evolve

Deleted: To ensure comparability of wind estimates at basin or global scales, such corrections should be clearly documented and incorporated into standard processing protocols for acoustic-equipped floats.

Formatted: English (UK)

Formatted: Font: Times New Roman, 12 pt, Font color: Auto, English (UK)

Deleted: By leveraging reanalysis products for first order fitting and applying localized corrections when available, our framework enables accurate, event-resolving wind estimates without the need for long-term surface infrastructure. Scaling this approach across the BGC-Argo array would provide high-resolution, all-weather wind monitoring in regions poorly served by existing networks.

1421 **4 Conclusions**

1422 This study provides a proof of concept for retrieving surface wind speeds from subsurface
 1423 ambient noise recorded by a profiling float equipped with a passive acoustic sensor and
 1424 operated alongside standard biogeochemical sensors. Float-measured acoustic noise captured
 1425 surface wind variability from 500–1000 m depth, and empirically calibrated estimates closely
 1426 matched buoy observations, confirming the feasibility of subsurface acoustic wind retrieval.
 1427 Reanalysis-based calibration reproduced moderate winds but underestimated high-wind
 1428 events, highlighting the limits of using reanalysis alone in dynamic environments. A residual-
 1429 learning correction using sparse local reference data substantially improved performance,
 1430 particularly during strong winds. These findings underscore the potential of acoustic-equipped
 1431 profiling floats to provide scalable, high-resolution wind observations in remote regions,
 1432 supporting improved estimates of wind-driven air-sea fluxes.

1433 Nevertheless, our results stem from a single short-duration deployment. Broader validation
 1434 across regions, seasons, and acoustic environments is needed, and performance estimates likely
 1435 represent an upper bound. Recent benchmarking efforts (e.g., Gros-Martial et al., 2025b) already
 1436 demonstrate the value of assembling multi-site acoustic-meteorological datasets and
 1437 highlight the challenges of model transferability across diverse soundscapes. Future missions
 1438 should employ independent training-validation-test partitions to rigorously evaluate
 1439 generalizability, following best practices established in recent WOTAN studies that explicitly
 1440 address temporal correlation and multi-site validation requirements (e.g., Cauchy et al., 2018;
 1441 Taylor et al., 2020; Trucco et al., 2022; Trucco et al., 2023).

1442 Acoustic wind retrieval offers a promising pathway for expanding autonomous wind
 1443 monitoring within the global BGC-Argo array, improving coverage in regions poorly served
 1444 by existing systems. Sparse in-situ calibration also provides a valuable new data stream for
 1445 validating and potentially correcting regional biases in global wind reanalyses. Ultimately, this
 1446 work supports the Ocean Sound EOVS's call for standardized methodologies and demonstrates
 1447 the feasibility of integrating passive acoustics into sustained, basin- to global-scale observing
 1448 systems.

1449

Deleted: ¶**Formatted:** Font: (Default) Times New Roman, 12 pt, Font color: Auto, English (UK)**Formatted:** Font: (Default) Times New Roman, 12 pt, Font color: Auto, English (UK)**Formatted:** Font: (Default) Times New Roman, 12 pt, Font color: Auto, English (UK)**Formatted:** Font: (Default) Times New Roman, 12 pt, Font color: Auto, English (UK)**Formatted:** Font: (Default) Times New Roman, 12 pt, Font color: Auto, English (UK)**Formatted:** Font: (Default) Times New Roman, 12 pt, Font color: Auto, English (UK)**Formatted:** Font: (Default) Times New Roman, 12 pt, Font color: Auto, English (UK)**Deleted:** This study provides the first demonstration of
 1450 retrieving surface wind speeds from subsurface ambient
 1451 noise recorded by a profiling float equipped with a passive
 1452 acoustic sensor. By integrating a low-power hydrophone
 1453 onto an autonomous profiling float and applying established
 1454 acoustic retrieval algorithms, we successfully detected
 1455 surface wind variability from depths between 500 and
 1456 1000 m. When empirically calibrated using collocated buoy
 1457 observations, float-derived wind speed estimates closely
 1458 matched in-situ surface measurements, confirming the
 1459 feasibility and accuracy of this approach under realistic
 1460 oceanographic conditions. ¶
 1461 To evaluate its potential for application in remote, data-
 1462 sparse regions, we simulated a scenario where acoustic
 1463 models were calibrated solely using ERA5 reanalysis winds.
 1464 Although the ERA5-based calibration captured moderate
 1465 wind variability effectively ($2.5\text{--}10 \text{ m s}^{-1}$), it consistently
 1466 underestimated high-wind events, underscoring limitations in
 1467 using reanalysis data as a standalone reference. To mitigate
 1468 this, we implemented a residual-learning approach,
 1469 leveraging brief periods of local wind observations (e.g.,
 1470 from ship-based or moored instruments) to correct
 1471 systematic errors in the acoustic estimates. This hybrid
 1472 methodology substantially improved model performance,
 1473 particularly under high-wind conditions, maintaining
 1474 accuracy across extended float trajectories and
 1475 demonstrating robustness for operational use. ¶
 1476 These findings underscore the potential of acoustic-equipped
 1477 profiling floats as scalable and autonomous platforms
 1478 capable of delivering high-resolution surface wind
 1479 observations in remote or poorly instrumented oceanic
 1480 regions. Such observations are particularly critical for
 1481 refining estimates of air-sea exchanges, including the
 1482 oceanic uptake and release of CO_2 , processes significantly
 1483 influenced by wind-driven gas exchange. Combined with
 1484 emerging biogeochemical proxy algorithms, such as
 1485 CANYON-B and CONTENT, acoustic-equipped floats can
 1486 now provide fully autonomous, integrated estimates of air-
 1487 sea CO_2 fluxes by coupling accurate wind measurements
 1488 with concurrent measurements of oceanic temperature,
 1489 salinity, and oxygen. ¶
 1490 Nevertheless, this study represents a single deployment in a
 1491 semi-enclosed basin. Broader validation across diverse
 1492 oceanographic regimes, including open-ocean gyres, polar
 1493 regions, and high-energy storm zones, is necessary to fully
 1494 assess the robustness, generalizability, and temporal stability
 1495 of the proposed correction frameworks. Future deployments
 1496 will help refine the methods presented here and furth... [38]

1579 **Funding.** The research leading to these results has received part of the funding from the
1580 European Union's Horizon research and innovation program under grants #101094716
1581 (GEORGE project) and #101188028 (TRICUSO project). REFINE has received funding from
1582 the European Research Council (ERC) under the European Union's Horizon 2020 research and
1583 innovation programme (grant agreement N° 834177). Argo-2030 has received the support of
1584 the French government within the framework of the "Investissements d'avenir" program
1585 integrated in France 2030 and managed by the Agence Nationale de la Recherche (ANR) under
1586 the reference "ANR-21-ESRE-0019".

1587 **Data availability.** The two deployments of this prototype float have not been assigned a WMO
1588 identifier and have not been declared in Argo; the data are therefore not available through the
1589 Argo program. All float data, DYFAMED buoy measurements, ERA5 reanalysis wind fields,
1590 and analysis scripts used in this study is freely available online [in Delaigue \(2025\)](#). The
1591 repository include processed datasets, code for model fitting and residual learning, and figure-
1592 generation scripts to ensure full reproducibility of results.

Deleted: at <https://doi.org/10.5281/zenodo.17232551>

1593 **Author contributions.** EL, HC, and LD conceptualized the project. AD and CS developed the
1594 acoustic sensor used in this study. LD curated the data. EL, HC, and LD performed the
1595 investigation. LD conceptualized the methodology, used the necessary software, visualized the
1596 data, and prepared the original draft of the paper. AGM, DC, EL, HC, JB, LD, PC, RB and SP
1597 reviewed and edited the paper.

1598 **Competing interests.** NKE instrumentation is a private company which commercialized the
1599 acoustic float, in which AD and CS are employed. The acoustic float is based on the PROVOR
1600 CTS5 platform and on an acoustic sensor developed and commercialized by NKE
1601 instrumentation with a partnership agreement with LOV. All other co-authors declare no
1602 competing interests.

1603 **Disclaimer.** Publisher's note: Copernicus Publications remains neutral with regard to
1604 jurisdictional claims in published maps and institutional affiliations.

1605 **Acknowledgements.** [We gratefully acknowledge the MOOSE team \(Mediterranean Ocean](#)
1606 [Observing System for the Environment\) at OSU STAMAR for their support in deploying the](#)
1607 [float, recovering it, and enabling its second deployment. We also thank the crew of the Téthys](#)
1608 [for their assistance at sea, and Jean-Yves for facilitating two successful float recoveries on short](#)
1609 [notice. We are grateful to Météo-France for maintaining and providing access to the Côte](#)
1610 [d'Azur meteorological buoy data at the DYFAMED site, which were essential for validating](#)
1611 [our wind measurements. We also acknowledge the MOOSE program \(Mediterranean Ocean](#)
1612 [Observing System for the Environment\), funded by CNRS-INSU, and the Research](#)
1613 [Infrastructure ILICO \(CNRS-IFREMER\) for their long-term support of sustained ocean](#)
1614 [observations in the northwestern Mediterranean. We further thank the European Centre for](#)
1615 [Medium-Range Weather Forecasts \(ECMWF\) for making the ERA5 reanalysis products freely](#)
1616 [available, which provided an essential reference dataset for this study. We thank Aldo Napoli](#)
1617 [\(Mines Paris\) for his assistance with the AIS data and Ambroise Renaud \(Mines Paris\) for](#)
1618 [making his modified version of libais freely available on GitHub, which allowed us to parse](#)
1619 [NMEA data from the AIS reception device at Mines Paris \(Sophia Antipolis\) and from the](#)
1620 [AISHub feed. Finally, we are grateful to AISHub \(AIS data sharing and vessel tracking\) for](#)
1621 [providing access to their AIS data services.](#)

Deleted: We gratefully acknowledge the MOOSE team (Mediterranean Ocean Observing System for the Environment) at OSU STAMAR for their support in deploying the float, recovering it, and enabling its second deployment. We also thank the crew of the Téthys for their assistance at sea, and Jean-Yves for facilitating two successful float recoveries on short notice. We are grateful to the European Centre for Medium-Range Weather Forecasts (ECMWF) for making the ERA5 reanalysis products freely available, which provided an essential reference dataset for this study. We also thank Aldo Napoli (Mines Paris) for his assistance with the AIS data and Ambroise Renaud (Mines Paris) for making his modified version of libais freely available on GitHub, which allowed us to parse NMEA data from the AIS reception device at Mines Paris (Sophia Antipolis) and from the AISHub feed. We are also grateful to AISHub (AIS data sharing and vessel tracking by AISHub) for providing access to their AIS data services.¶

1642 **References**

1643 Baumgartner, M. F., Stafford, K. M., and Latha, G.: Near real-time underwater passive acoustic
1644 monitoring of natural and anthropogenic sounds, in: *Observing the Oceans in Real Time*, 203–
1645 226, 2017.

1646 Baumgartner, M. F. and Bonnel, J.: Real-time detection and classification of marine mammals
1647 from expendable profiling floats, Workshop on Detection, Classification, Localization and
1648 Density Estimation of Marine Mammals using Passive Acoustics, Oahu, USA, March 2022.

1649 Bell, B., Hersbach, H., Simmons, A., Berrisford, P., Dahlgren, P., Horányi, A., Muñoz-Sabater,
1650 J., Nicolas, J., Radu, R., Schepers, D., and Thépaut, J.-N.: The ERA5 global reanalysis:
1651 Preliminary extension to 1950, *Q. J. Roy. Meteor. Soc.*, 147, 4186–
1652 4227, <https://doi.org/10.1002/qj.4174>, 2021.

1653 Bentamy, A., Katsaros, K. B., Mestas-Nuñez, A. M., Drennan, W. M., Forde, E. B., and
1654 Roquet, H.: Satellite estimates of wind speed and latent heat flux over the global oceans, *J.
1655 Climate*, 16, 637–656, [https://doi.org/10.1175/1520-0442\(2003\)016<0637:SEOWSA>2.0.CO;2](https://doi.org/10.1175/1520-0442(2003)016<0637:SEOWSA>2.0.CO;2), 2003.

1656 Bushinsky, S. M., Gray, A. R., Johnson, K. S., and Sarmiento, J. L.: Oxygen in the Southern
1657 Ocean from Argo floats: Determination of processes driving air–sea fluxes, *J. Geophys. Res.-
1658 Oceans*, 122, 8661–8682, <https://doi.org/10.1002/2017JC012923>, 2017.

1659 Bytheway, J. L., Thompson, E. J., Yang, J., and Chen, H.: Evaluating satellite precipitation
1660 estimates over oceans using passive aquatic listeners, *Geophys. Res. Lett.*, 50,
1661 [e2022GL102087](https://doi.org/10.1029/2022GL102087), <https://doi.org/10.1029/2022GL102087>, 2023.

1662 Cauchy, P., Heywood, K. J., Merchant, N. D., Queste, B. Y., and Testor, P.: Wind speed
1663 measured from underwater gliders using passive acoustics, *J. Atmos. Ocean. Technol.*, 35,
1664 2305–2321, <https://doi.org/10.1175/JTECH-D-17-0209.1>, 2018.

1665 Cauchy, P., Heywood, K. J., Risch, D., Merchant, N. D., Queste, B. Y., and Testor, P.: Sperm
1666 whale presence observed using passive acoustic monitoring from gliders of opportunity,
1667 *Endang. Species Res.*, 42, 133–149, <https://doi.org/10.3354/esr01044>, 2020.

1668 Cazau, D., Bonnel, J., and Baumgartner, M. F.: Wind speed estimation using an acoustic
1669 underwater glider in a near-shore marine environment, *IEEE Trans. Geosci. Remote Sens.*, 57,
1670 2097–2106, <https://doi.org/10.1109/TGRS.2018.2871422>, 2019.

1671 Cazau, D., Bonnel, J., Jouma'a, J., Le Bras, Y., and Guinet, C.: Measuring the marine
1672 soundscape of the Indian Ocean with southern elephant seals used as acoustic gliders of
1673 opportunity, *J. Atmos. Ocean. Technol.*, 34, 207–223, <https://doi.org/10.1175/JTECH-D-16-0124.1>, 2017.

1674 Chelton, D. B., Schlax, M. G., Samelson, R. M., and de Szoeke, R. A.: Global observations of
1675 large oceanic eddies, *Geophys. Res. Lett.*, 34,
1676 L15606, <https://doi.org/10.1029/2007GL030812>, 2007.

1679 Chen, T. and Guestrin, C.: XGBoost: A scalable tree boosting system, Proc. 22nd ACM
1680 SIGKDD Int. Conf. Knowl. Discov. Data Min., 785–
1681 794, <https://doi.org/10.1145/2939672.2939785>, 2016.

1682 Claustre, H., Johnson, K. S., and Takeshita, Y.: Observing the global ocean with
1683 Biogeochemical-Argo, *Annu. Rev. Mar. Sci.*, 12, 23–48, <https://doi.org/10.1146/annurev-marine-010419-010956>, 2020.

1685 Cocquempot, L., Delacourt, C., Paillet, J., Riou, P., Aucan, J., Castelle, B., Charria, G., Claudet,
1686 J., Conan, P., Coppola, L., Hocdé, R., Planes, S., Raimbault, P., Savoye, N., Testut, L., and
1687 Vuillemin, R.: Coastal Ocean and Nearshore Observation: A French Case Study, *Front. Mar.
1688 Sci.*, 6, 324, <https://doi.org/10.3389/fmars.2019.00324>, 2019.

1689 Delaigue, L. (2025). *louisdelague/WIND-FROM-FLOAT-ACOUSTICS*: Initial release for
1690 Zenodo DOI (v1.1). Zenodo. <https://doi.org/10.5281/zenodo.17232552>

1691 D'ortenzo, F., Taillandier, V., Claustre, H., et al.: Biogeochemical Argo: The test case of the
1692 NAOS Mediterranean array, *Front. Mar. Sci.*, 7, 120, <https://doi.org/10.3389/fmars.2020.00120>, 2020.

1694 Dotto, T. S., Naveira Garabato, A. C., Bacon, S., et al.: Wind-driven processes controlling
1695 oceanic heat delivery to the Amundsen Sea, Antarctica, *J. Phys. Oceanogr.*, 49, 2829–
1696 2849, <https://doi.org/10.1175/JPO-D-19-0064.1>, 2019.

1697 Farmer, D. M., Vagle, S., and Booth, A. D.: A free-flooding acoustical resonator for
1698 measurement of bubble size distributions, *J. Atmos. Ocean. Technol.*, 15, 1132–
1699 1146, [https://doi.org/10.1175/1520-0426\(1998\)015<1132:AFFARF>2.0.CO;2](https://doi.org/10.1175/1520-0426(1998)015<1132:AFFARF>2.0.CO;2), 1998.

1700 Fregosi, S., Harris, D. V., Matsumoto, H., Mellinger, D. K., Barlow, J., Baumann-Pickering,
1701 S., and Klinck, H.: Detections of whale vocalizations by simultaneously deployed bottom-
1702 moored and deep-water mobile autonomous hydrophones, *Front. Mar. Sci.*, 7,
1703 721, <https://doi.org/10.3389/fmars.2020.00721>, 2020.

1704 Gray, A. R., Johnson, K. S., Bushinsky, S. M., et al.: Autonomous biogeochemical floats detect
1705 significant carbon dioxide outgassing in the high-latitude Southern Ocean, *Geophys. Res. Lett.*,
1706 45, 9049–9057, <https://doi.org/10.1029/2018GL078013>, 2018.

1707 Gros-Martial, A., Dubus, G., Cazau, D., Bazin, S., and Guinet, C.: Producing a new in-situ
1708 wind speed product for the Southern Ocean based on acoustic meteorology from biologged
1709 southern elephant seals, *J. Atmos. Ocean. Technol.*, <https://doi.org/10.1175/JTECH-D-25-0037.1>, 2025a.

1711 Gros-Martial, A., Delaigue, L., Cauchy, P., Pensieri, S., Bozzano, R., Bonnel, J., Leymarie, E.,
1712 Baumgartner, M., Guinet, C., Bazin, S., and Cazau, D.: Benchmarking models for ocean wind
1713 speed estimation based on passive acoustic monitoring, *OCEANS 2025 Brest*, Brest, France,
1714 IEEE, 1–10, <https://doi.org/10.1109/OCEANS58557.2025.11104747>, 2025b.

1715 Gruber, N., Bakker, D. C. E., DeVries, T., et al.: Trends and variability in the ocean carbon
1716 sink, *Nat. Rev. Earth Environ.*, 4, 119–134, <https://doi.org/10.1038/s43017-022-00381-x>,
1717 2023.

1718 Ingenito, F. and Wolf, S. N.: Site dependence of wind-dominated ambient noise in shallow
1719 water, *J. Acoust. Soc. Am.*, 85, 141–145, <https://doi.org/10.1121/1.397722>, 1989.

1720 Johnson, K. S. and Claustre, H.: Bringing biogeochemistry into the Argo age, *Eos Trans. AGU*,
1721 97, <https://doi.org/10.1029/2016EO062427>, 2016.

1722 Li, Z., Thompson, E. J., Behrangi, A., Chen, H., and Yang, J.: Performance of GPCP daily
1723 products over oceans: Evaluation using Passive Aquatic Listeners, *Geophys. Res. Lett.*, 50,
1724 e2023GL104310, <https://doi.org/10.1029/2023GL104310>, 2023.

1725 Ma, B. B. and Nystuen, J. A.: Prediction of underwater sound levels from rain and wind, *J.*
1726 *Acoust. Soc. Am.*, 117, 3555–3565, <https://doi.org/10.1121/1.1910283>, 2005.

1727 Ma, B. B., Girton, J. B., Dunlap, J. H., Gobat, J. I., and Chen, J.: Passive acoustic measurements
1728 on autonomous profiling floats, *OCEANS 2023 – MTS/IEEE U.S. Gulf Coast*, Biloxi, USA,
1729 1–6, <https://doi.org/10.23919/OCEANS52994.2023.10337032>, 2023.

1730 Matsumoto, H., Jones, C., Klinck, H., et al.: Tracking beaked whales with a passive acoustic
1731 profiler float, *J. Acoust. Soc. Am.*, 133, 731–740, <https://doi.org/10.1121/1.4773260>, 2013.

1732 McGillicuddy, D. J.: Mechanisms of physical–biological–biogeochemical interaction at the
1733 oceanic mesoscale, *Annu. Rev. Mar. Sci.*, 8, 125–159, <https://doi.org/10.1146/annurev-marine-010814-015606>, 2016.

1735 McMonigal, K., Larson, S. M., and Gervais, M.: Wind-driven ocean circulation changes can
1736 amplify future cooling of the North Atlantic warming hole, *J. Climate*, 38, 2479–
1737 2496, <https://doi.org/10.1175/JCLI-D-24-0227.1>, 2025.

1738 Menze, S., Kindermann, L., van Opzeeland, I., et al.: Soundscapes of the Southern Ocean:
1739 Passive acoustic monitoring in the Weddell Sea, Conference presentation, 2013.

1740 Nystuen, J. A.: Listening to raindrops from underwater: an acoustic disdrometer, *J. Atmos.*
1741 *Ocean. Technol.*, 18, 1640–1657, [https://doi.org/10.1175/1520-0426\(2001\)018<1640:LTRFUA>2.0.CO;2](https://doi.org/10.1175/1520-0426(2001)018<1640:LTRFUA>2.0.CO;2), 2001.

1743 Nystuen, J. A., Anagnostou, M. N., Anagnostou, E. N., and Papadopoulos, A.: Monitoring
1744 Greek seas using passive underwater acoustics, *J. Atmos. Ocean. Technol.*, 32, 334–
1745 349, <https://doi.org/10.1175/JTECH-D-13-00264.1>, 2015.

1746 Oguz, H. N. and Prosperetti, A.: Bubble entrainment by the impact of drops on liquid surfaces,
1747 *J. Fluid Mech.*, 219, 143–179, <https://doi.org/10.1017/S0022112090002890>, 1990.

1748 Pelichero, V., Boutin, J., Claustre, H., Merlivat, L., Sallée, J.-B., and Blain, S.: Relaxation of
1749 wind stress drives the abrupt onset of biological carbon uptake in the Kerguelen bloom: a
1750 multisensor approach, *Geophys. Res. Lett.*, 47, 47,
1751 e2019GL085992, <https://doi.org/10.1029/2019GL085992>, 2020.

1752 Pensieri, S., Bozzano, R., Nystuen, J. A., Anagnostou, E. N., Anagnostou, M. N., and Bechini,
1753 R.: Underwater acoustic measurements to estimate wind and rainfall in the Mediterranean Sea,
1754 *Adv. Meteorol.*, 2015, 612512, <https://doi.org/10.1155/2015/612512>, 2015.

1755 Pipatprathanporn, S. and Simons, F. J.: One year of sound recorded by a MERMAID float in
1756 the Pacific: hydroacoustic earthquake signals and infrasonic ambient noise, *Geophys. J. Int.*,
1757 228, 193–212, <https://doi.org/10.1093/gji/ggab296>, 2022.

1758 Prawirasasra, M. S., Mustonen, M., and Klauson, A.: Wind fetch effect on underwater wind-
1759 driven sound, *Est. J. Earth Sci.*, 73, 15–25, <https://doi.org/10.3176/earth.2024.02>, 2024.

1760 Rainaud, R., Bouin, M.-N., Redelsperger, J.-L., et al.: Characterization of air-sea exchanges
1761 over the western Mediterranean Sea during HyMeX SOP1 using the AROME-WMED model,
1762 *Q. J. Roy. Meteor. Soc.*, 142, 173–187, <https://doi.org/10.1002/qj.2480>, 2016.

1763 Riser, S. C., Nystuen, J. A., and Rogers, A.: Monsoon effects in the Bay of Bengal inferred
1764 from profiling float-based measurements of wind speed and rainfall, *Limnol. Oceanogr.*, 53,
1765 2080–2093, https://doi.org/10.4319/lo.2008.53.5_part_2.2080, 2008.

1766 Riser, S. C., Freeland, H. J., Roemmich, D., et al.: Fifteen years of ocean observations with
1767 the global Argo array, *Nat. Clim. Change*, 6, 145–153, <https://doi.org/10.1038/nclimate2872>,
1768 2016.

1769 Roemmich, D., G.C. Johnson, S. Riser, R. Davis, J. Gilson, W.B. Owens, S.L. Garzoli, C.
1770 Schmid, and M. Ignaszewski. The Argo Program: Observing the global ocean with profiling
1771 floats. *Oceanography* 22(2):34–43, <https://doi.org/10.5670/oceanog.2009.36>, 2009.

1772 Schwock, F. and Abadi, S.: Statistical analysis and modeling of underwater wind noise at the
1773 northeast Pacific continental margin, *J. Acoust. Soc. Am.*, 150, 4166–
1774 4177, <https://doi.org/10.1121/10.0007463>, 2021.

1775 Stoffelen, A., Portabella, M., Verhoef, A., Verspeek, J., and Vogelzang, J.: High-resolution
1776 ASCAT scatterometer winds near the coast, *IGARSS 2008 – IEEE Int. Geosci. Remote Sens.*
1777 Symp., Boston, USA, 7–11 July 2008, I-114–I-
1778 117, <https://doi.org/10.1109/IGARSS.2008.4778806>, 2008.

1779 Taylor, W. O., Anagnostou, M. N., Cerrai, D., and Anagnostou, E. N.: Machine learning
1780 methods to approximate rainfall and wind from acoustic underwater measurements, *IEEE*
1781 *Trans. Geosci. Remote Sens.*, 59, 2810–2821, <https://doi.org/10.1109/TGRS.2020.3007557>,
1782 2021.

1783 Trenberth, K. E., Cheng, L., Pan, Y., Fasullo, J., and Mayer, M.: Distinctive pattern of global
1784 warming in ocean heat content, *J. Climate*, 38, 2155–2168, [https://doi.org/10.1175/JCLI-D-24-0609.1](https://doi.org/10.1175/JCLI-D-24-
1785 0609.1), 2025.

1786 Trucco, A., Barla, A., Bozzano, R., Pensieri, S., and Repetto, S.: Compounding approaches for
1787 wind prediction from underwater noise by supervised learning, *IEEE J. Oceanic Eng.*, 47,
1788 1172–1187, <https://doi.org/10.1109/JOE.2022.3162689>, 2022.

1789 Trucco, A., Barla, A., Bozzano, R., Pensieri, S., and Repetto, S.: Introducing temporal
1790 correlation in rainfall and wind prediction from underwater noise, *IEEE J. Oceanic Eng.*, 48,
1791 349–364, <https://doi.org/10.1109/JOE.2022.3223406>, 2023.

1792 Tyack, P., Akamatsu, T., Boebel, O., Chapuis, L., Debusschere, E., de Jong, C., Erbe, C.,
1793 Evans, K., Gedamke, J., Gridley, T., Haralabus, G., Jenkins, R., Miksis-Olds, J., Sagen, H.,
1794 Thomsen, F., Thomisch, K., and Urban, E.: Ocean Sound Essential Ocean Variable
1795 Implementation Plan, Zenodo [data set], <https://doi.org/10.5281/zenodo.10067187>, 2023.

1796 Vagle, S., Large, W. G., and Farmer, D. M.: An evaluation of the WOTAN technique of
1797 inferring oceanic winds from underwater ambient sound, *J. Atmos. Ocean. Technol.*, 7, 576–
1798 595, [https://doi.org/10.1175/1520-0426\(1990\)007<0576:AEOTWT>2.0.CO;2](https://doi.org/10.1175/1520-0426(1990)007<0576:AEOTWT>2.0.CO;2), 1990.

1799 Wang, Y., Yao, Q., Kwok, J. T., and Ni, L. M.: Generalizing from a few examples: A survey
1800 on few-shot learning, *ACM Comput. Surv.*, 53, 1–34, <https://doi.org/10.1145/3386252>, 2020.

1801 Wanninkhof, R.: Relationship between wind speed and gas exchange over the ocean revisited,
1802 *Limnol. Oceanogr.-Meth.*, 12, 351–362, <https://doi.org/10.4319/lom.2014.12.351>, 2014.

1803 Wanninkhof, R., Triñanes, J., Pierrot, D., et al.: Trends in sea–air CO₂ fluxes and sensitivities
1804 to atmospheric forcing using an extremely randomized trees machine learning approach, *Glob.*
1805 *Biogeochem. Cycles*, 39, e2024GB008315, <https://doi.org/10.1029/2024GB008315>, 2025.

1806 Yang, J., Riser, S. C., Nystuen, J. A., Asher, W. E., and Jessup, A. T.: Regional rainfall
1807 measurements using the Passive Aquatic Listener during the SPURS field campaign,
1808 *Oceanography*, 28, 124–133, <https://doi.org/10.5670/oceanog.2015.10>, 2015.

1809 Yang, J., Asher, W. E., and Riser, S. C.: Rainfall measurements in the North Atlantic Ocean
1810 using underwater ambient sound, in: 2016 IEEE/OES China Ocean Acoustics (COA), Harbin,
1811 China, 9–11 January 2016, 1–4, <https://doi.org/10.1109/COA.2016.7535834>, 2016.

1812 Zambra, M., Cazau, D., Farrugia, N., Gensse, A., Pensieri, S., Bozzano, R. and Fablet,
1813 R.: Learning-based temporal estimation of in-situ wind speed from underwater passive
1814 acoustics, *IEEE J. Oceanic Eng.*, 48, 1215–1225, <https://doi.org/10.1109/JOE.2023.3288970>,
1815 2023.

1816 Zhang, M., Cheng, Y., Bao, Y., Zhao, C., Wang, G., Zhang, Y., Song, Z., Wu, Z., and Qiao,
1817 F.: Seasonal to decadal spatiotemporal variations of the global ocean carbon sink, *Glob.*
1818 *Change Biol.*, 28, 1786–1797, <https://doi.org/10.1111/gcb.16031>, 2022.

Page 2: [1] Deleted	Louise Delaigue	11/25/25 1:32:00 PM
---------------------	-----------------	---------------------

.....

Page 2: [2] Deleted	Louise Delaigue	11/17/25 11:54:00 AM
---------------------	-----------------	----------------------

.....

Page 2: [3] Deleted	Louise Delaigue	11/17/25 11:55:00 AM
---------------------	-----------------	----------------------

.....

Page 2: [4] Deleted	Louise Delaigue	11/25/25 3:43:00 PM
---------------------	-----------------	---------------------

.....

Page 2: [5] Formatted	Louise Delaigue	11/25/25 1:36:00 PM
-----------------------	-----------------	---------------------

Font: Times New Roman, 12 pt, Font color: Auto, English (UK)

Page 2: [6] Formatted	Louise Delaigue	11/25/25 1:36:00 PM
-----------------------	-----------------	---------------------

Font: Times New Roman, 12 pt, Font color: Auto, English (UK)

Page 2: [7] Formatted	Louise Delaigue	11/25/25 1:36:00 PM
-----------------------	-----------------	---------------------

Font: Times New Roman, 12 pt, Font color: Auto, English (UK)

Page 2: [8] Deleted	Louise Delaigue	11/17/25 11:56:00 AM
---------------------	-----------------	----------------------

.....

Page 3: [9] Deleted	Louise Delaigue	11/25/25 1:37:00 PM
---------------------	-----------------	---------------------

.....

Page 3: [10] Deleted	Louise Delaigue	11/17/25 12:00:00 PM
----------------------	-----------------	----------------------

.....

Page 3: [11] Deleted	Louise Delaigue	11/17/25 12:02:00 PM
----------------------	-----------------	----------------------

.....

Page 3: [12] Deleted	Louise Delaigue	11/17/25 12:03:00 PM
----------------------	-----------------	----------------------

.....

Page 3: [13] Deleted	Louise Delaigue	11/17/25 12:03:00 PM
----------------------	-----------------	----------------------

.....

Page 14: [14] Deleted	Louise Delaigue	11/17/25 3:24:00 PM
-----------------------	-----------------	---------------------

.....

Page 20: [15] Formatted	Louise Delaigue	11/17/25 3:56:00 PM
-------------------------	-----------------	---------------------

Default Paragraph Font, Font color: Auto, English (UK)

Page 20: [15] Formatted	Louise Delaigue	11/17/25 3:56:00 PM
-------------------------	-----------------	---------------------

Default Paragraph Font, Font color: Auto, English (UK)

Page 20: [15] Formatted	Louise Delaigue	11/17/25 3:56:00 PM
-------------------------	-----------------	---------------------

Default Paragraph Font, Font color: Auto, English (UK)

Page 20: [16] Deleted

Louise Delaigue

11/25/25 1:56:00 PM

▼

Page 20: [16] Deleted

Louise Delaigue

11/25/25 1:56:00 PM

▼

Page 20: [16] Deleted

Louise Delaigue

11/25/25 1:56:00 PM

▼

Page 20: [16] Deleted

Louise Delaigue

11/25/25 1:56:00 PM

▼

Page 20: [16] Deleted

Louise Delaigue

11/25/25 1:56:00 PM

▼

Page 20: [16] Deleted

Louise Delaigue

11/25/25 1:56:00 PM

▼

Page 20: [16] Deleted

Louise Delaigue

11/25/25 1:56:00 PM

▼

Page 20: [16] Deleted

Louise Delaigue

11/25/25 1:56:00 PM

▼

Page 20: [16] Deleted

Louise Delaigue

11/25/25 1:56:00 PM

▼

Page 20: [16] Deleted

Louise Delaigue

11/25/25 1:56:00 PM

▼

Page 20: [16] Deleted

Louise Delaigue

11/25/25 1:56:00 PM

Page 20: [17] Deleted

Louise Delaigue

11/17/25 3:58:00 PM

Page 20: [17] Deleted

Louise Delaigue

11/17/25 3:58:00 PM

Page 20: [17] Deleted

Louise Delaigue

11/17/25 3:58:00 PM

Page 20: [17] Deleted

Louise Delaigue

11/17/25 3:58:00 PM

Page 20: [17] Deleted

Louise Delaigue

11/17/25 3:58:00 PM

Page 20: [17] Deleted

Louise Delaigue

11/17/25 3:58:00 PM

Page 20: [17] Deleted

Louise Delaigue

11/17/25 3:58:00 PM

Page 20: [17] Deleted

Louise Delaigue

11/17/25 3:58:00 PM

Page 20: [18] Formatted

Louise Delaigue

11/17/25 3:59:00 PM

Font: Times New Roman, 12 pt, Font color: Auto, English (UK)

Page 20: [18] Formatted

Louise Delaigue

11/17/25 3:59:00 PM

Font: Times New Roman, 12 pt, Font color: Auto, English (UK)

Page 20: [19] Deleted

Louise Delaigue

11/17/25 4:00:00 PM

Page 20: [20] Deleted

Louise Delaigue

11/17/25 4:00:00 PM

Page 20: [20] Deleted

Louise Delaigue

11/17/25 4:00:00 PM

Page 20: [20] Deleted

Louise Delaigue

11/17/25 4:00:00 PM

Page 20: [20] Deleted

Louise Delaigue

11/17/25 4:00:00 PM

Page 20: [20] Deleted

Louise Delaigue

11/17/25 4:00:00 PM

Page 20: [21] Formatted

Louise Delaigue

11/17/25 4:01:00 PM

Default Paragraph Font, Font color: Auto, English (UK)

Page 20: [21] Formatted

Louise Delaigue

11/17/25 4:01:00 PM

Default Paragraph Font, Font color: Auto, English (UK)

Page 20: [22] Formatted

Louise Delaigue

11/17/25 4:02:00 PM

Default Paragraph Font, Font color: Auto, English (UK)

Page 20: [22] Formatted

Louise Delaigue

11/17/25 4:02:00 PM

Default Paragraph Font, Font color: Auto, English (UK)

Page 20: [22] Formatted

Louise Delaigue

11/17/25 4:02:00 PM

Default Paragraph Font, Font color: Auto, English (UK)

Page 20: [23] Deleted

Louise Delaigue

11/17/25 4:02:00 PM

Page 20: [24] Deleted

Louise Delaigue

11/17/25 4:03:00 PM

Page 20: [24] Deleted

Louise Delaigue

11/17/25 4:03:00 PM

Page 20: [25] Deleted

Louise Delaigue

11/17/25 4:03:00 PM

Page 20: [25] Deleted

Louise Delaigue

11/17/25 4:03:00 PM

Page 20: [25] Deleted

Louise Delaigue

11/17/25 4:03:00 PM

Page 20: [25] Deleted

Louise Delaigue

11/17/25 4:03:00 PM

Page 20: [25] Deleted

Louise Delaigue

11/17/25 4:03:00 PM

Page 20: [25] Deleted

Louise Delaigue

11/17/25 4:03:00 PM

Page 20: [25] Deleted

Louise Delaigue

11/17/25 4:03:00 PM

Page 20: [25] Deleted

Louise Delaigue

11/17/25 4:03:00 PM

Page 20: [25] Deleted

Louise Delaigue

11/17/25 4:03:00 PM

Page 20: [25] Deleted

Louise Delaigue

11/17/25 4:03:00 PM

Page 20: [25] Deleted

Louise Delaigue

11/17/25 4:03:00 PM

Page 21: [26] Deleted

Louise Delaigue

11/17/25 4:08:00 PM

Page 21: [27] Formatted

Louise Delaigue

11/17/25 4:10:00 PM

Font: Times New Roman, 12 pt, Font color: Auto, English (UK)

Page 21: [28] Formatted

Louise Delaigue

11/17/25 4:10:00 PM

Default Paragraph Font, Font color: Auto, English (UK)

Page 21: [29] Formatted

Louise Delaigue

11/17/25 4:10:00 PM

Font: Times New Roman, 12 pt, Font color: Auto, English (UK)

Page 21: [30] Deleted

Louise Delaigue

11/17/25 4:10:00 PM

Page 21: [31] Deleted

Louise Delaigue

11/17/25 4:11:00 PM

Page 21: [32] Deleted

Louise Delaigue

11/17/25 4:12:00 PM

Page 21: [33] Deleted

Louise Delaigue

11/17/25 4:12:00 PM

Page 22: [34] Deleted

Louise Delaigue

11/17/25 4:15:00 PM

Page 22: [35] Deleted

Louise Delaigue

11/17/25 4:17:00 PM

Page 22: [36] Deleted

Louise Delaigue

11/17/25 4:17:00 PM

Page 22: [37] Deleted

Louise Delaigue

11/17/25 4:18:00 PM

Page 24: [38] Deleted

Louise Delaigue

11/17/25 4:26:00 PM

|

▼

